Quantum computing & Quantum information

Bachelor thesis
Microtechnology and Nanoscience - MCCX02
May 19, 2010

Authors:

Tommy Andersson	(tommya@student.chalmers.se)
Håkan Carlsson	(hakanc@student.chalmers.se)
Anders Martinsson	(anders.martinsson@chalmers.se)
Ida-Maria Svensson	(idamaris@student.chalmers.se)
Tobias Wenger	(wenger@student.chalmers.se)

Supervisors:

Göran Johansson	(goran.l.johansson@chalmers.se)
Chris Wilson	(chris.wilson@chalmers.se)

Abstract

This report is an introduction to quantum computation and quantum information. We present a two-part theory section followed by data analysis of a transmon qubit. The first theory part, needed for the analysis, introduces fundamental properties of qubit states and the Bloch sphere description. The qubit manipulation, interaction with a electromagnetic field, is then studied in the Rabi model (semi-classical) and the Jaynes-Cummings model (fully quantized). The second theory part is a qualitative presentation of the density matrix representation, decoherence (effects of noise) and read-out, which are useful topics in more advanced analysis.

We also present a summary of qubit realizations, with focus on the superconducting qubits: charge, phase and transmon.

In the last part of the report, we analyze spectroscopic measurements on a transmon qubit in a cavity resonator, performed at MC2 Chalmers. The data was compared to the expected behavior from the Jaynes-Cummings Hamiltonian and then the full Hamiltonian for the transmon. The comparison enabled us to extract the parameters of the transmon. The ratio of the Josephson energy and the charge energy was determined to be $E_J/E_C = 34.5644 \pm 0.9456$ GHz, which is in the transmon regime. Furthermore, the coupling strength between the cavity resonator and the qubit was determined to be $2\beta e V^0_{rms} = 0.1301 \pm 0.00095$ GHz, with a 68 % confidence interval.

Contents

1 Introduction & Objective

Recent development in microtechnology and nanofabrication has allowed accurate construction of electrical circuits in the nanometer range. As the spatial dimension of the circuits decreases to this regime, quantum effects become apparent. In some applications these effects are limiting, but for our concerns, they are fundamental properties to be taken advantage of.

This project has been devoted to the study of one particular realization of a quantum bit (qubit), the transmon, which is basically a small superconducting circuit placed in a cavity resonator. The transmon is currently used in research at MC2 Chalmers.

To get familiar with the field of nanoscience and microtechnology, in particularly quantum computing and quantum information, all project participants attended the course *Quantum Informatics (FKA 172)* during the first quarter of 2010. As this field of study was relatively new to us, a major part of our work has consisted of literature studies, to provide the necessary knowledge. In section 3 and 4 we present the theory retrieved throughout the course.

At the end of the course, our supervisors provided experimental data from microwave spectroscopy of a transmon qubit in a cavity resonator. With this data, our task was to determine energy levels of the system. To do this, we performed simulations using models discussed during the course Quantum Informatics. The outcome of these simulations is the highlight of our work, since understanding of the theory is required to implement it into executable code and evaluate the obtained results. Finally, the simulations were compared with the experimental data and we could determine the characteristic parameters of the transmon.

The aim has been to produce a report in the field of quantum computing and quantum information understandable for a student, who has taken introductory courses in quantum physics, e.g. the undergraduate quantum physics courses in Engineering Physics at Chalmers. For the student it is necessary to read theory - part I to be able to understand the work we have done with simulating the transmon. Theory - part II introduces some concepts vital for further studies in the subject, however these are not used in the data analysis.

2 Background

The computer has undergone a tremendous development in recent decades. The development has followed Moore's Law (1965), which states that the number of transistors that can be placed on an integrated chip has doubled every two years. This has mainly been done by shrinking the size of transistors, but the circuits are now so small, that quantum effects begin to interfere.

In 1982, Richard Feynman pointed out the problem with simulating larger quantum systems using classical computers and suggested a computer based on quantum principles. A few years later, in 1985, David Deutsch made a significant contribution when he constructed the theoretical model of the universal quantum computer. He showed that it could solve all kinds of problems that a classical computer could solve. Theoretically the opposite also holds, any algorithm that can run on a quantum computer can be simulated on a classical computer. However, many phenomena which are fundamental for a quantum system such as superposition and quantum entanglement do not have any simple equivalent on a classical computer. Because of that, the amount of time and memory needed to simulate a quantum computer will grow exponentially as the number of quantum bits increases.

The development of quantum computing and quantum information gained speed, when in 1995, Peter Shor showed that the problem of finding prime factors of an integer could be solved efficiently on a quantum computer [1]. This is important because a commonly used encryption algorithm, RSA, is based on the fact that finding prime factors of large integers is believed to have no efficient solution on a classical computer [2].

What Feynman theorized about and David Deutsch showed was that quantum computing enables a more powerful way of doing computations. Instead of doing calculation after calculation, all possible outcomes can exist in a superposition. In figure 1 we see a simple example, where "quantum parallelism" is visualized as checking all positions in a registry simultaneously.

Figure 1: An example of how a quantum computer can be faster than a classical computer is the problem to search through an unsorted database. A classical computer (left) has to evaluate each leaf separatly while a quantum computer (right) can evaluate all leaves simultaneously as a superposition. Courtesy of [3].

Although quantum physics has been around for roughly a century, there are fundamental questions as well as practical difficulties with the realization of qubits. The present problem is to get the qubits to work coherently for more than short periods of time. Thus, the main obstacle is decoherence, the interaction between the qubit and its environment, which causes the qubit to lose its quantum characteristics and thus also its ability to perform quantum computing. However, in just ten years, the timescale in which a qubit behaves coherently, has increased with three orders of magnitude. Even though quantum

computers have the potential to become more powerful than their classical counterparts, the current research is still far from this point.

In 1999, Nakamura et al. induced Rabi oscillations in a single-Cooper-pair box, which was an important outcome of 20 years of thorough research in superconducting circuits [4]. In the recent ten years, coherent control and Rabi oscillations have been observed also in flux qubits and phase qubits [5]. In 2007, Koch et al. suggested a combination of the charge qubit and the phase qubit, the transmon qubit, which might be a suitable candidate for quantum computing [6].

Worth mentioning, apart from the qubit application, is that quantum circuits are of great interest also for research in fundamental physics. With use of these circuits it is possible to explore interactions at a very fundamental level not previously achievable. Experiments studying the interaction between an artificial atom in a cavity and a single photon is an example where the quantum circuits have opened up new experimental regimes.

3 Theory - Part I

The theory presented (both part I and part II) is mainly, but not exclusively, the content of the course Quantum Informatics. In turn, the course is based on *Quantum Computing and Quantum Information* [2] and *Introductory Quantum Optics* [7]. References are explicitly displayed, when information and statements used in section 3 and 4 are not retrieved from either of these two books.

Initially, we introduce quantum two-level systems, bra-ket notation and single qubit dynamics, which are necessary to understand the basic properties of a qubit. To visualize qubit states and qubit operations, the Bloch sphere is then discussed. Thereafter, the interaction between an artificial atom (a qubit) and the electromagnetic field is described. First, we consider the Rabi model, which is interaction between a classical field and an atom. Then, we describe how the electromagnetic field can be quantized, which leads to a full quantum mechanical description of the interaction. This quantized model is known as the Jaynes-Cummings model. Arriving at the Jaynes-Cummings Hamiltonian is the highlight of the theory survey, since we have used it to simulate the energy levels of the transmon.

The concepts introduced in this section are useful when treating an isolated quantum system, where the influence of the environment is neglected. To account for more advanced dynamics such as dissipation, the concepts discussed in section 4 are needed. However, since we could neglect decoherence in our analysis, the sufficient theory for understanding the data analysis of the transmon (section 6) is presented in this section.

3.1 Introduction to Quantum Computing

The basic building block in a conventional computer is the logical bit that is either 1 or 0. In the quantum computer the building block is the quantum bit. Classically, it can be in one of two states, ψ_0 or ψ_1. However, a fundamental property of quantum mechanical systems is the superposition of states, which means that any state $\alpha\psi_0 + \beta\psi_1$ is possible, with α,$\beta \in \mathbb{C}$ such that $|\alpha|^2 + |\beta|^2 = 1$. To perform quantum computing, the dynamics of the system should be limited to these states. When a measurement is performed, the wave function collapses and the qubit will be measured to be in either ψ_0, with probability $|\alpha|^2$ or ψ_1, with probability $|\beta|^2$.

A quantum state can be described by a wave function $\psi(x,t)$, where the time evolution of the state is governed by the time-dependent Schrödinger equation

$$i\hbar\partial_t\psi(x,t) = \hat{H}\psi(x,t).$$

$\hat{H}$ is the Hamiltonian and describes the total energy of the system. From the time-independent Schrödinger equation

$$\hat{H}\psi_n(x,t) = E_n\psi_n(x,t)$$

the eigenstates ψ_0, ψ_1,... can be obtained. The eigenstates represent energy levels E_n and for some quantum mechanical systems, which are potential qubits, it is possible to limit the dynamics to a two-level system ψ_0, ψ_1. Then the total wave function can be written

$$\psi(x,t) = c_0(t)\psi_0(x) + c_1(t)\psi_1(x),$$

where the dynamics of the system is represented by the time-dependent coefficients. If the states ψ_0 and ψ_1 are normalized and orthogonal, the probability to measure one of the states is given by $P_{0/1}(t) = |c_{0/1}(t)|^2$. The wave function formalism is clear, but when extending to more energy levels there exists a more practical notation.

The influence from a time-dependent Hamiltonian acting on a the wave function can be written as

$$\begin{aligned}\hat{H}(t)\psi(x,t) &= \hat{H}(t)(c_0(t)\psi_0(x) + c_1(t)\psi_1(x)) \\ &= c_0(t)(h_{00}(t)\psi_0(x) + h_{10}(t)\psi_1(x)) + c_1(t)(h_{01}(t)\psi_0(x) + h_{11}(t)\psi_1(x)),\end{aligned}$$

where the coefficients h_{ij} can be interpreted as matrix elements. This gives an interpretation of the Hamiltonian as a matrix, $\hat{H} = \begin{pmatrix} h_{00} & h_{01} \\ h_{10} & h_{11} \end{pmatrix}$ and the state as a vector $\psi = \begin{pmatrix} c_0 \\ c_1 \end{pmatrix}$, defining ψ_0 as $\begin{pmatrix} 1 \\ 0 \end{pmatrix}$ and ψ_1 as $\begin{pmatrix} 0 \\ 1 \end{pmatrix}$ as the basis for the system. The matrix elements in $\hat{H}$ can be calculated as

$$h_{ij} = \int \psi_i^*(x)\hat{H}(t)\psi_j(x)dx.$$

From linear algebra, we know that any linear operator acting on the system can be represented by a matrix.

Qubit states are vectors in a two dimensional Hilbert space, spanned by the base vectors. The explicit matrix notation works for a single qubit but when controlling more qubits, the size of the matrices is growing exponentially. A N-qubit system requires 2^N-dimensional vectors. Hence the vector notation becomes tedious. The Dirac notation using bra's and ket's provides a more convenient way to represent states.

In Dirac notation the qubit state ψ can be written

$$|\psi\rangle = c_0|0\rangle + c_1|1\rangle,$$

where the kets represents the two eigenstates ψ_0 and ψ_1. The corresponding bra vector can be written as $(|\psi\rangle)^\dagger = (c_0|0\rangle + c_1|1\rangle)^\dagger = c_0^*\langle 0| + c_1^*\langle 1| = \langle\psi|$, which can be interpreted as taking the transpose and complex conjugate of the state. More details about Dirac notation can be found in Sakurai [8].

In Dirac notation $\langle\phi|\theta\rangle = \int \phi^*(x)\theta(x)dx$ represents the inner product between $|\phi\rangle$ and $|\theta\rangle$ and can be interpreted as the scalar product between the state vectors. From this notation it can easily be seen that the base vectors $|0\rangle = \begin{pmatrix} 1 \\ 0 \end{pmatrix}$ and $|1\rangle = \begin{pmatrix} 0 \\ 1 \end{pmatrix}$ preserve the fundamental properties normalization

$$\langle 0|0\rangle = \begin{pmatrix} 1 & 0 \end{pmatrix} \begin{pmatrix} 1 \\ 0 \end{pmatrix} = 1,$$

orthogonality

$$\langle 0|1\rangle = \begin{pmatrix} 1 & 0 \end{pmatrix} \begin{pmatrix} 0 \\ 1 \end{pmatrix} = 0$$

and completeness

$$|0\rangle\langle 0| + |1\rangle\langle 1| = \hat{\mathbf{1}},$$

where $\hat{\mathbf{1}}$ is the identity operator.

In the general case completeness is written as

$$\sum_i |i\rangle\langle i| = \hat{\mathbf{1}},$$

where i forms an arbitrary basis. Using this condition, an operator X can be represented as

$$X = \sum_i \sum_j |i\rangle\langle i|X|j\rangle\langle j|.$$

Since i and j are vectors of equal length N the operator matrix will be N×N with i indicating row and j indicating column as $X_{ij} = \langle i|X|j\rangle$. It should now be clear that qubit states can be represented using either Dirac or vector notation and that operators can be represented as matrices.

To be noted is the abbreviated notation $|\phi\rangle|\theta\rangle$ for the tensor product, which should actually be written as $|\phi\rangle \otimes |\theta\rangle$. A full description of the properties of tensor products are beyond the scope of this report, however from the matrix representation it has an easy interpretation as the Kronecker product. For more details about tensor products see Appendix A.

3.2 The Bloch Sphere

When considering a single qubit, the Bloch sphere is a way to visualize different states of the system. The Bloch sphere is a unit sphere where qubit states are represented by points on the surface. The point on the top of the sphere corresponds to the state $|0\rangle$ and the bottom to the state $|1\rangle$. Generally, the latitude of a point corresponds to the probability to measure the qubit to be in $|0\rangle$ or $|1\rangle$. The longitude represents the phase difference between the terms $|0\rangle$ and $|1\rangle$ in the state.

Let $|\psi\rangle = \alpha|0\rangle + \beta|1\rangle$ be a qubit state. α and β can be written on polar form, $\alpha = r_\alpha e^{i\varphi_\alpha}$ $\beta = r_\beta e^{i\varphi_\beta}$. This gives

$$|\psi\rangle = r_\alpha e^{i\varphi_\alpha}|0\rangle + r_\beta e^{i\varphi_\beta}|1\rangle = e^{i\varphi_\alpha}\left(r_\alpha|0\rangle + r_\beta e^{i(\varphi_\beta - \varphi_\alpha)}\right).$$

Because of the fact that the overall phase is not observable, we can simplify the expression for $|\psi\rangle$ by discarding the factor $e^{i\varphi_\alpha}$,

$$|\psi'\rangle = r_\alpha|0\rangle + r_\beta e^{i(\varphi_\beta - \varphi_\alpha)}|1\rangle.$$

Now, the idea is to express $|\psi'\rangle$ in terms of spherical coordinates, φ and θ. As described above, the phase difference between the two eigenstates corresponds to φ, and thus we put $\varphi_\beta - \varphi_\alpha = \varphi$. The angle θ should correspond to the values of r_α and r_β. By normalization, $r_\alpha^2 + r_\beta^2 = 1$. Further, when $\theta = 0$, $r_\alpha = 1$ and $r_\beta = 0$ and vice versa when $\theta = \pi$. This implies the relation $r_\alpha = \cos\frac{\theta}{2}$ and $r_\beta = \sin\frac{\theta}{2}$.

The transformation results in the Bloch sphere, see figure 2, where the point corresponding to the state $|\psi\rangle$ is expressed in spherical coordinates θ and φ. After the transformation a

general qubit state on the Bloch sphere can be written as [9]

$$|\psi'(\theta,\varphi)\rangle = \cos\frac{\theta}{2}|0\rangle + \sin\frac{\theta}{2}e^{i\varphi}|1\rangle, \qquad (3.2.1)$$
$$0 \leq \theta \leq \pi,$$
$$0 \leq \varphi \leq 2\pi.$$

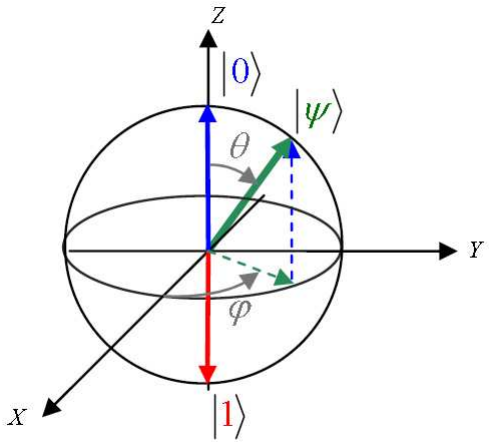

Figure 2: An illustration of the Bloch sphere. Courtesy of [10].

The idea of the Bloch sphere comes from the behaviour of spin 1/2-particles, such as electrons and many atomic nuclei. The quantum states for the spin of such a particle forms a two-level system where its state can be written as a superposition of the spin up and spin down states. In this case, the points on the Bloch sphere correspond to the direction of the spin. We now consider the Pauli matrices which plays an important role in this picture, the three Pauli matrices are

$$\sigma_x = \begin{pmatrix} 0 & 1 \\ 1 & 0 \end{pmatrix}, \sigma_y = \begin{pmatrix} 0 & -i \\ i & 0 \end{pmatrix} \text{ and } \sigma_z = \begin{pmatrix} 1 & 0 \\ 0 & -1 \end{pmatrix}.$$

Using the result of equation (3.2.1) it is possible to examine their expectation values

$$\langle\hat{\sigma}_x\rangle = \langle\psi'(\theta,\varphi)|\sigma_x|\psi'(\theta,\varphi)\rangle = 2\sin\frac{\theta}{2}\cos\frac{\theta}{2}\frac{(e^{i\varphi}+e^{-i\varphi})}{2} = \sin\theta\cos\varphi, \quad (3.2.2a)$$
$$\langle\hat{\sigma}_y\rangle = \langle\psi'(\theta,\varphi)|\sigma_y|\psi'(\theta,\varphi)\rangle = 2\sin\frac{\theta}{2}\cos\frac{\theta}{2}\frac{(e^{i\varphi}-e^{-i\varphi})}{2i} = \sin\theta\sin\varphi, \quad (3.2.2b)$$
$$\langle\hat{\sigma}_z\rangle = \langle\psi'(\theta,\varphi)|\sigma_z|\psi'(\theta,\varphi)\rangle = \cos^2\frac{\theta}{2} - \sin^2\frac{\theta}{2} = \cos\theta, \quad (3.2.2c)$$

which is nothing more than the state projected on the respective axis of the matrices. This is important because any two-by-two dimensional matrix can be written in terms of the Pauli matrices which means that any two-by-two dimensional Hamiltonian can be expressed as actions on the qubit state vector on the Bloch sphere, by a fictitious magnetic field.

To perform qubit operations there must be a way to interact with the qubit and it is convenient to picture the state vector time evolution on the Bloch sphere. In the Hamiltonian formalism it is also convenient to write the energy in terms of the scalar product between the magnetic dipole moment and a fictitious magnetic field. In the presence of an arbitrary magnetic field $B(t)$, the single qubit Hamiltonian is

$$\hat{H} = -\frac{1}{2}(B_x(t)\hat{\sigma}_x + B_y(t)\hat{\sigma}_y + B_z(t)\hat{\sigma}_z), \tag{3.2.3}$$

and if considering a magnetic field with only a z-component so that $B(t) = B_z(t)\hat{\sigma}_z$ the calculations are much easier to carry out. The Schrödinger equation for the system is

$$i\hbar \begin{pmatrix} \dot{c_0}\ (t) \\ \dot{c_1}\ (t) \end{pmatrix} = -\frac{1}{2}B_z(t)\hat{\sigma}_z \begin{pmatrix} c_0(t) \\ c_1(t) \end{pmatrix}$$

and these are just two uncoupled differential equations with the solution

$$\begin{pmatrix} c_0(t) \\ c_1(t) \end{pmatrix} = \begin{pmatrix} e^{\frac{i\delta}{2}} & 0 \\ 0 & e^{-\frac{i\delta}{2}} \end{pmatrix} \begin{pmatrix} c_0(0) \\ c_1(0) \end{pmatrix}, \tag{3.2.4}$$

$$\delta = \frac{1}{\hbar}\int_0^t dt' B_z(t').$$

Now, writing the time evolution operator

$$R_z(-\delta) = \begin{pmatrix} e^{\frac{i\delta}{2}} & 0 \\ 0 & e^{-\frac{i\delta}{2}} \end{pmatrix},$$

it is easy to see that

$$R_z(-\delta)|\psi'(\theta,\varphi)\rangle = |\psi'(\theta,\varphi-\delta)\rangle,$$

which means that a magnetic field along the z-axis has the effect of rotating the state vector around said axis with the angle $-\delta$. Since the z-axis is chosen arbitrarily it is easy to see that this applies for all directions; a magnetic field has the effect of rotating the state vector of the qubit around the axis of the field. In the case of an arbitrary magnetic field in the $\hat{n} = n_x\hat{x} + n_y\hat{y} + n_z\hat{z}$ direction where $|\hat{n}| = 1$ the time evolution operator becomes

$$R_{\hat{n}} = e^{i\frac{\delta}{2}(n_x\hat{\sigma}_x + n_y\hat{\sigma}_y + n_z\hat{\sigma}_z)} = \cos\frac{\delta}{2}\hat{\mathbf{1}} - i\sin\frac{\delta}{2}(n_x\hat{\sigma}_x + n_y\hat{\sigma}_y + n_z\hat{\sigma}_z),$$

where the last equality comes from simple series expansion of the exponential.

In reality, the energy difference between the two states ($|1\rangle$ and $|0\rangle$) $E_1 - E_0 = \hbar\omega_0$ corresponds to a term $-\frac{1}{2}\hbar\omega_0\hat{\sigma}_z$ in the Hamiltonian (3.2.3), which can be seen as a strong fictitious magnetic field in the z-direction. Any qubit state will thus precess quickly around the z-axis with angular frequency ω_0.

Defining the Hamiltonian ΔH describing the dynamics, the Hamiltonian for the qubit is rewritten to:

$$\hat{H} = -\frac{1}{2}\hbar\omega_0\hat{\sigma}_z + \Delta\hat{H}.$$

The description of the dynamics can be simplified by using a coordinate system rotating along with the precession. This transforms the state vector to

$$|\psi'\rangle = R_z(\omega_0 t)|\psi\rangle$$

and the Hamiltonian to

$$\hat{H}' = R_z(\omega_0 t)\Delta\hat{H}R_z(-\omega_0 t).$$

Notice that the term $-\frac{1}{2}\hbar\omega_0\hat{\sigma}_z$ vanishes, leaving only the dynamics of the system $\Delta\hat{H}$. This transformation is called the rotating frame [3].

3.3 Qubit Manipulation and Atom-field Interactions

In order to perform calculations with qubits, different gates need to be implemented. According to the Bloch sphere description, two rotations around two non-parallell axes are required to put the qubit in an arbitrary state. As the vector on the Bloch sphere precesses around the z-axis due to energy spacing the only additional operation needed is changing the population. The natural method to do this is to apply small harmonic perturbations, and was first introduced by Rabi [11] when he worked on nuclear magnetic resonance.

To describe qubit manipulations, consider a quantum mechanical system of an electron bound to an atomic nucleus. A qubit can be considered as an artificial atom, though the calculations in this section regard an electron, the results can also be applied to a qubit. The Hamiltonian for this system in absence of external fields is

$$\hat{H}_0 = \frac{1}{2m}\hat{\mathbf{p}}^2 + V(r), \tag{3.3.1}$$

where $V(r)$ is the Coulomb potential, $r = |\mathbf{r}|$ is the distance between the nucleus and the electron and $\hat{\mathbf{p}} = -i\hbar\nabla$ is the momentum operator. When an external electromagnetic field with the vector potential $\mathbf{A}(\mathbf{r},t)$ and the scalar potential $\phi(\mathbf{r},t)$ is applied, the Hamiltonian is changed to [12]

$$\hat{H}(\mathbf{r},t) = \frac{1}{2m}[\hat{\mathbf{p}} + e\mathbf{A}(\mathbf{r},t)]^2 - e\phi(\mathbf{r},t) + V(r),$$

where e is the elementary charge. The electric and the magnetic fields are given by Maxwell's equations and can be expressed by the scalar potential ϕ and the vector potential $\mathbf{A}$ as

$$\mathbf{E}(\mathbf{r},t) = -\nabla\phi(\mathbf{r},t) - \partial_t\mathbf{A}(\mathbf{r},t),$$
$$\mathbf{B}(\mathbf{r},t) = \nabla \times \mathbf{A}(\mathbf{r},t).$$

The electromagnetic field is invariant under gauge transformations. When performing Gauge transformations to a solution in classical electromagnetism, it means that Maxwell's equations are still satisfied. The potentials can be rewritten as

$$\phi'(\mathbf{r},t) = \phi(\mathbf{r},t) - \partial_t\chi(\mathbf{r},t), \tag{3.3.2a}$$
$$\mathbf{A}'(\mathbf{r},t) = \mathbf{A}(\mathbf{r},t) + \nabla\chi(\mathbf{r},t), \tag{3.3.2b}$$

where $\chi(\mathbf{r},t)$ is an arbitrary scalar field (see Appendix B for transformation details).

To simplify calculations a definite choice of gauge, namely the Coulomb (also known as the transverse or radiation) gauge can be used. Applying this $\nabla \cdot \mathbf{A} = 0$ and $\phi = 0$. Using this, the radiation field is completely described by the vector potential $\mathbf{A}$. With the transformations given by (3.3.2), the Hamiltonian becomes

$$\hat{H}'(\mathbf{r},t) = \frac{1}{2m}[\hat{\mathbf{p}} + e(\mathbf{A}(\mathbf{r},t) + \nabla\chi(\mathbf{r},t))]^2 + e\partial_t\chi(\mathbf{r},t) + V(r). \tag{3.3.3}$$

This expression can be simplified even more using the properties of the vector potential. Without any charge sources near the atom, the vector potential satisfies the wave equation

$$\nabla^2 \mathbf{A} - \frac{1}{c}\partial_t^2 \mathbf{A} = 0.$$

The solutions to this equation are plane-waves on the form

$$\mathbf{A} = \mathbf{A}_0 e^{i(\mathbf{k}\cdot\mathbf{r}-\omega t)} + \text{constant},$$

where the $|\mathbf{k}| = 2\pi/\lambda$ is the wave vector of the radiation and λ the wavelength. An approximation that will simplify calculations is the dipole approximation. If the spatial extension of the atom, $|\mathbf{r}|$ (typically a few Ångströms) is much smaller than the wavelength λ of the radiation (hundreds of nanometers), thus $\mathbf{k}\cdot\mathbf{r} \ll 1$, the spatial dependence of the vector potential can be neglected, $\mathbf{A}(\mathbf{r},t) \simeq \mathbf{A}(t)$. The arbitrary scalar function can now be chosen to $\chi(\mathbf{r},t) = -\mathbf{A}(t)\cdot\mathbf{r}$. This gives

$$\nabla\chi(\mathbf{r},t) = -\mathbf{A}(t),$$

$$\partial_t\chi(\mathbf{r},t) = -\mathbf{r}\cdot\partial_t\mathbf{A}(t) = \mathbf{r}\cdot\mathbf{E}(t),$$

where Maxwell's equations once again are used. Using this choice of χ the Hamiltonian given by equation (3.3.3) can be simplified

$$\hat{H}'(\mathbf{r},t) = \frac{1}{2m}\hat{\mathbf{p}}^2 + V(r) + e\mathbf{r}\cdot\mathbf{E}(t) = \hat{H}_0 - \hat{\mathbf{d}}\cdot\mathbf{E}(t). \tag{3.3.4}$$

This Hamiltonian describes the interaction between the applied field and the atom within the dipole-approximation, where $-e\mathbf{r} = \hat{\mathbf{d}}$ is called the dipole operator. The dipole operator is a measure of charge separation and determines how strongly the qubit interacts with the field within the dipole approximation. This derivation of the Hamiltonian is fortunately valid for both classical and quantized electromagnetic fields, because the nature of the electromagnetic field is not specified.

3.4 The Rabi Model

The Rabi model describes interaction between a classical electromagnetic field and an atom with two energy levels. This will induce coherent control, i.e it is possible to put the system in a arbitrary state. The model is labeled as semi-classical, because the nature of the field is not considered to be quantized, as it would be in fully quantum mechanical description, section 3.6, but is still useful for a qualitative understanding.

In order to calculate the time-evolution of an atom in an electromagnetic field, it has to be assumed that the field is near resonance with the atomic state transition. An implication of the assumption is that the field will induce transitions and perturbation theory can not describe the time-evolution. Thus, the problem has to be solved more "exactly".

The two atomic levels, with different parity, are the ground state $|g\rangle$ and the excited state $|e\rangle$. The transition frequency between the two states is

$$\omega_0 = \frac{1}{\hbar}(E_e - E_g).$$

Then a harmonic electromagnetic field is applied, $\mathbf{E}(t) = \mathbf{E}_0 \cos \omega t$, with a frequency near resonance for atomic state transition, $|\omega - \omega_0| \ll \omega_0$ and $\mathbf{E}_0$ is the electric field pointing in an arbitrary direction. The Hamiltonian for the system will be, using equation (3.3.4)

$$\hat{H} = \hat{H}_0 + \hat{V}_0 \cos \omega t, \tag{3.4.1}$$

where $\hat{V}_0 = -\hat{\mathbf{d}} \cdot \mathbf{E}_0$. The state vector of the two-level system can be written as

$$|\psi\rangle = C_g(t) e^{iE_g t/\hbar} |g\rangle + C_e(t) e^{iE_e t/\hbar} |e\rangle.$$

Then the time-dependent Schrödinger equation with the Hamiltonian from equation (3.4.1) will give

$$i\hbar \partial_t |\psi\rangle = \left(\hat{H}_0 + \hat{V}_0 \cos \omega t\right) |\psi\rangle.$$

Multiplication of both sides with $\langle g|$ and $\langle e|$ gives a system of coupled differential equations for the amplitudes C_g and C_e

$$\dot{C}_g = -\frac{i}{\hbar} \vartheta \cos \omega t e^{-i\omega_0 t} C_e, \tag{3.4.2a}$$

$$\dot{C}_e = -\frac{i}{\hbar} \vartheta \cos \omega t e^{i\omega_0 t} C_g, \tag{3.4.2b}$$

where $\vartheta = \langle e|\hat{V}_0|g\rangle$. Here we have used that $\langle g|\hat{V}_0|g\rangle = \langle e|\hat{V}_0|e\rangle = 0$ due to parity. Then equations (3.4.2) can be rewritten by using $\cos \phi = (e^{i\phi} + e^{-i\phi})/2$, which gives expressions $e^{\pm i(\omega+\omega_0)t}$ and $e^{\pm i(\omega-\omega_0)t}$. By the initial assumption that the frequency of the electromagnetic field is near resonance with atomic transition, $e^{\pm i(\omega+\omega_0)t}$ will oscillate so fast they will average out on the timescale considered, hence they can be neglected. This is also called Rotating Wave Approximation [13]. Using this approximation together with equations (3.4.2) yields

$$\dot{C}_g = -\frac{i}{2\hbar} \vartheta e^{i(\omega-\omega_0)t} C_e,$$

$$\dot{C}_e = -\frac{i}{2\hbar} \vartheta e^{-i(\omega-\omega_0)t} C_g.$$

This can be solved as a differential equation of order two

$$\ddot{C}_e + i(\omega - \omega_0)\dot{C}_e + \frac{1}{4}\frac{\vartheta^2}{\hbar^2} C_e = 0.$$

Using initial conditions where $C_g(0) = 1$ and $C_e(0) = 0$, i.e. the system is in the ground state

$$C_e(t) = -i\frac{\vartheta}{\Omega_R \hbar} e^{i\Delta t/2} \sin \Omega_R t/2, \tag{3.4.4a}$$

$$C_g(t) = e^{i\Delta t/2} \left[\cos \Omega_R t/2 - i\frac{\Delta}{\Omega_R} \sin \Omega_R t/2\right], \tag{3.4.4b}$$

where the detuning $\Delta = \omega_0 - \omega$ and the Rabi frequency

$$\Omega_R = \sqrt{\Delta^2 + \left(\frac{\vartheta}{\hbar}\right)^2}$$

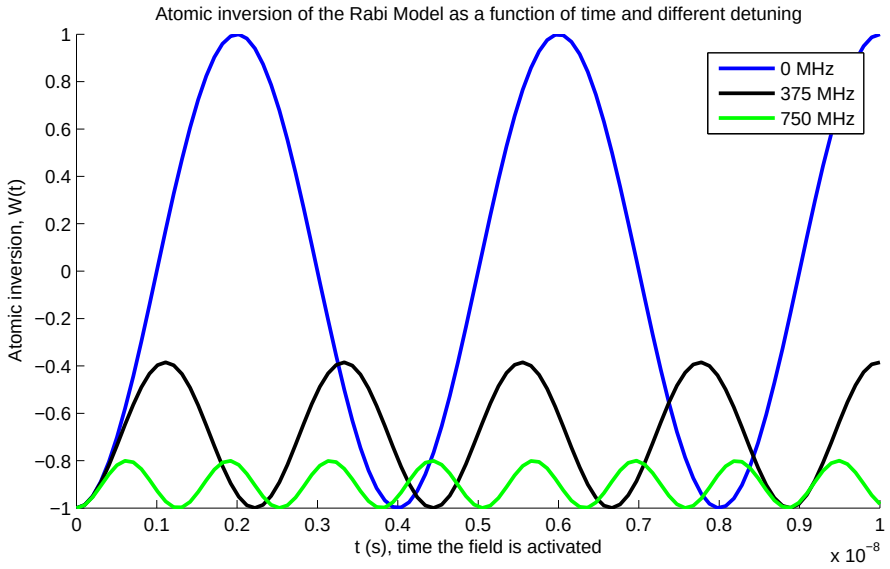

Figure 3: Atomic inversion $W(t) = P_e(t) - P_g(t)$, or minus the projection on z-axis in the Bloch sphere description induced by Rabi oscillations. $W(t)$ is plotted for different detuning as a function of the time. The detuning is $\Delta = 0{,}375{,}750$ MHz for the plots in descending order, i.e smaller amplitude for bigger detuning.

are introduced. The probability for the atom to be in the ground state and excited state are

$$P_e(t) = |C_e(t)|^2 = \left(\frac{\vartheta}{\Omega_R \hbar} \sin \Omega_R t/2\right)^2$$

and

$$P_g(t) = |C_g(t)|^2 = (\cos \Omega_R t/2)^2 + \left(\frac{\Delta}{\Omega_R} \sin \Omega_R t/2\right)^2$$

respectively.

It is useful to consider the atomic inversion, or minus the z-projection on the Bloch sphere

$$W(t) = P_e(t) - P_g(t), \tag{3.4.5}$$

which is plotted in figure 3, the so called Rabi oscillations for different detuning can be seen. At exact resonance ($\Delta = 0$), (3.4.5) is reduced to

$$W(t) = \sin^2 \frac{\vartheta t}{2\hbar} - \cos^2 \frac{\vartheta t}{2\hbar} = -\cos \frac{\vartheta t}{\hbar}.$$

After $t = \pi\hbar/\vartheta$ all the atomic population has been transferred to the excited state, $W(\pi\hbar/\vartheta) = 1$. This is called a π pulse, because on the Bloch sphere, the vector for the state is rotated by π radians. Using this it is matter of adjusting t to put the atom in an arbitrary state. For instance, let $t = \pi\hbar/2\vartheta$. This yields

$$C_e(\pi\hbar/2\vartheta) = \frac{i}{\sqrt{2}},$$

$$C_g(\pi\hbar/2\vartheta) = \frac{1}{\sqrt{2}}.$$

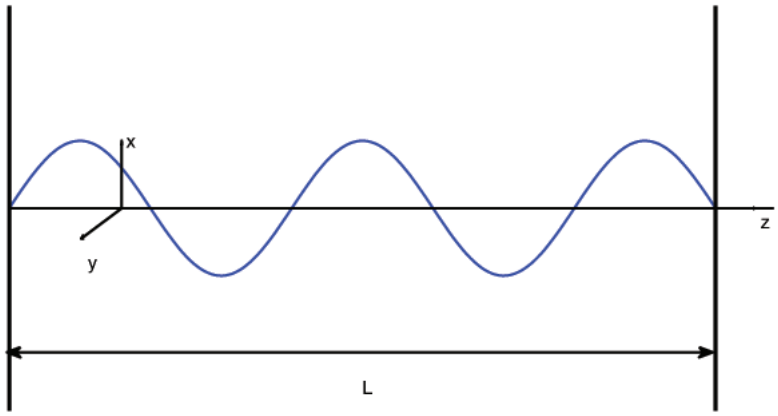

Figure 4: Schematic figure of the one dimensional cavity resonator. In z-direction it has length L, and infinite length in x- and y-direction.

3.5 Quantization of the Electromagnetic Field

In the previous section the electromagnetic field was classical and lead to a qualitative understanding of how to change the state of the qubit. But in order to get a fully quantum mechanical description of the qubit manipulation, the field has to be quantized as well.

Consider a one dimensional cavity, see figure 4, along the z-axis with perfectly conducting walls at $z = 0$ and $z = L$. When having these boundary conditions the electric field vanishes at the boundaries. Assuming that there are no charges or currents present in the system, Maxwell's equations are [14]

$$\nabla \times \mathbf{E} = -\partial_t \mathbf{B}, \tag{3.5.1a}$$
$$\nabla \times \mathbf{B} = \mu_0 \epsilon_0 \partial_t \mathbf{E}, \tag{3.5.1b}$$
$$\nabla \cdot B = 0, \tag{3.5.1c}$$
$$\nabla \cdot E = 0. \tag{3.5.1d}$$

Further assuming that the electric field is polarized along the x-axis and in a single mode, $\mathbf{E}(\mathbf{r},t) = \mathbf{e}_x E_x(z,t)$, the solution to (3.5.1) is

$$E_x(z,t) = \sqrt{\frac{2\omega_m^2}{V\epsilon_0}} q(t) \sin(kz), \tag{3.5.2a}$$
$$B_y(z,t) = \left(\frac{\mu_o \epsilon_0}{k}\right) \sqrt{\frac{2\omega_m^2}{V\epsilon_0}} \dot{q}(t) \cos(kz), \tag{3.5.2b}$$

where $\omega_m = c(m\pi/L)$ is the frequency of the mode and m takes the values $m = 1,2,\ldots$ to satisfy the boundary conditions. The cavity is consequently called a cavity resonator, as only certain frequencies and wave numbers $k_m = \omega_m/c$ forms standing waves. Also in (3.5.2) there is the effective volume of the cavity $V = A_{cav}L$, where A_{cav} is the area of

the cavity resonator. The time-dependent factor $q(t)$ of dimension length is introduced and used later. The magnetic field is polarized in the y-direction, $\mathbf{B}(\mathbf{r},t) = \mathbf{e}_y B_y(z,t)$.

Then, writing down the classical field energy, or Hamiltonian H, of the electromagnetic field gives

$$H = \frac{1}{2}\int dV \left[\epsilon_0 \mathbf{E}^2(\mathbf{r},t) + \frac{1}{\mu_0}\mathbf{B}^2(\mathbf{r},t)\right] = \frac{1}{2}(\dot{q}^2 + \omega^2 q^2). \tag{3.5.3}$$

Now by identifying terms in the Hamiltonian (3.5.3), we can see that it is the classical harmonic oscillator with unit mass. By introducing canonical variables $p = \dot{q}$ and q as momentum and position operators and imposing the canonical commutation relation

$$[\hat{q},\hat{p}] = i\hbar,$$

the Hamiltonian (3.5.3) can describe the quantized field. The new operators are Hermitian and therefore observable, but it is more convenient to introduce the annihilation ($\hat{a}$) and creation ($\hat{a}^\dagger$) operators

$$\hat{a} = \frac{1}{\sqrt{2\hbar\omega_m}}(\omega_m \hat{q} + i\hat{p}), \tag{3.5.4a}$$

$$\hat{a}^\dagger = \frac{1}{\sqrt{2\hbar\omega_m}}(\omega_m \hat{q} - i\hat{p}). \tag{3.5.4b}$$

Now the electric and magnetic field (3.5.2) can be rewritten in terms of the new operators (3.5.4)

$$\hat{E}_x(z,t) = \varepsilon_0(\hat{a} + \hat{a}^\dagger)\sin(kz), \tag{3.5.5a}$$

$$\hat{B}_y(z,t) = \beta_0(\hat{a} - \hat{a}^\dagger)\cos(kz), \tag{3.5.5b}$$

where $\varepsilon_0 = \sqrt{\hbar\omega_m/\epsilon_0 V}$ and $\beta_0 = (\mu_0/k)\sqrt{\epsilon_0\hbar\omega_m^3/V}$ and represents the electric and magnetic fields "per photon" respectively. This is not entirely true and since the expectation values of these fields are zero, see [7] for details, but are nevertheless useful measures of the fluctuations of the quantized field. The creation and annihilation operators satisfy the commutation relation

$$[\hat{a},\hat{a}^\dagger] = 1$$

and transforms the Hamiltonian (3.5.3) to

$$\hat{H} = \hbar\omega_m\left(\hat{a}^\dagger\hat{a} + \frac{1}{2}\right). \tag{3.5.6}$$

The eigenstates for this Hamiltonian are the number eigenstates of the harmonic oscillator, and here represents the number of photons in the cavity, denoted by

$$|n\rangle = \frac{(\hat{a}^\dagger)^n}{\sqrt{n!}}|0\rangle.$$

The operators (3.5.4) has the properties:

$$\hat{a}^\dagger|n\rangle = \sqrt{n+1}\;|n+1\rangle, \tag{3.5.7a}$$

$$\hat{a}|n\rangle = \sqrt{n}\;|n-1\rangle. \tag{3.5.7b}$$

The term $\hat{a}^\dagger\hat{a}$ is also known as the number operator $\hat{n}$, and comes from

$$\hat{a}^\dagger\hat{a}|n_c\rangle = \sqrt{n_c}a^\dagger|n_c - 1\rangle = n_c|n_c\rangle = \hat{n}_c|n_c\rangle. \tag{3.5.8}$$

Although this quantization only holds for the electromagnetic field in a one dimensional cavity for a single mode, the method for generalizing to higher dimensions and multiple modes is analogues. The solutions to Maxwell's equations (3.5.1) will still be on the same form.

To get the matrix representation of the operators for the quantized field the completeness relation has to be used and is further developed in section 6.2.

3.6 Jaynes-Cummings Hamiltonian

The Jaynes-Cummings Hamiltonian describes the dynamics of a qubit coupled to an electromagnetic field just as the Rabi Hamiltonian, see equation (3.4.1). The difference is that the Jaynes-Cummings model accounts for the quantized nature of the electromagnetic field. The field is restricted to a cavity resonator, which is essentially just a "one-dimensional" waveguide so the derivation in section 3.5 is valid for the Hamiltonian of the field. Another important restriction is that the qubit is assumed to have only two levels, $|g\rangle$ and $|e\rangle$. This simplifies matters and makes it possible to express the Hamiltonian in terms of Pauli matrices.

The entire Hamiltonian can be broken down in three different parts and be written as

$$\hat{H} = \hat{H}_0 + \hat{H}_F + \hat{H}_I, \tag{3.6.1}$$

where $\hat{H}_F$ is the Hamiltonian for the field in the cavity resonator from equation (3.5.6), $\hat{H}_0$ is the Hamiltonian for the qubit and $\hat{H}_I$ is the interaction between the cavity resonator and the qubit. The qubit Hamiltonian is the same as in the Rabi model, but the interaction part of the Hamiltonian becomes rather different. There also appears the new term which belongs to the field and has no analogue in the Rabi Hamiltonian. In vacuum, i.e. zero photons in the cavity resonator, the eigenvalue of the number operator is zero and the remaning term in equation (3.5.6) $\frac{\hbar\omega}{2}$, which is the zero point energy. However, the zero point energy does not contribute to the dynamics of the system, because the zero-level of the energy can be chosen arbitrarily, so the Hamiltonian for the electromagnetic field can be written as

$$\hat{H}_F = \hbar\omega\hat{a}^\dagger\hat{a}, \tag{3.6.2}$$

if the zero point energy term is dropped.

For the qubit, we can define the zero-level of the energy to be in the middle of $|g\rangle$ and $|e\rangle$ and the qubit Hamiltonian is written as

$$\hat{H}_0 = -\frac{1}{2}\hbar\omega_0\hat{\sigma}_z. \tag{3.6.3}$$

This is a big simplification as it approximates the qubit as a general two level system.

In order to write down the interaction Hamiltonian it is convenient to first introduce some new operators. The atomic transition operators are

$$\begin{aligned} \hat{\sigma}_+ &= |e\rangle\langle g|, \\ \hat{\sigma}_- &= |g\rangle\langle e| = \hat{\sigma}_+^\dagger. \end{aligned} \tag{3.6.4}$$

The $\hat{\sigma}_+$ and $\hat{\sigma}_-$ excites and deexcites the qubit respectively and it is easy to show that

$$\hat{\sigma}_+|g\rangle = |e\rangle,$$
$$\hat{\sigma}_-|e\rangle = |g\rangle.$$

Under the assumption that the wavelength is much larger than the qubit, the dipole approximation is valid. The interaction Hamiltonian is then written on the same form as in equation (3.3.4)

$$\hat{H}_I = -\hat{\mathbf{d}} \cdot \hat{\mathbf{E}} = \hat{d}\lambda(\hat{a} + \hat{a}^\dagger), \tag{3.6.5}$$

where $\hat{\mathbf{E}}$ is the electric field as in equation (3.5.5) and λ is defined as the quantity $\lambda = -\left(\frac{\hbar\omega}{\epsilon_0 V}\right)^{1/2} \sin(kz)$. Now consider $\hat{d} = \hat{\mathbf{d}} \cdot \mathbf{e}$ which is the electric dipole moment operator. With use of the atomic transition operators, $\hat{d}$ can be simplified. Since by parity $\langle g|\hat{d}|g\rangle = \langle e|\hat{d}|e\rangle = 0$ it is possible to write $\hat{d} = d|g\rangle\langle e| + d^*|e\rangle\langle g|$ and under the assumption d is real obtain

$$\hat{d} = d(\hat{\sigma}_+ + \hat{\sigma}_-). \tag{3.6.6}$$

Now defining $g = \frac{d\lambda}{\hbar}$, which is the coupling between qubit and cavity resonator and using this result the interaction Hamiltonian can be written as

$$\hat{H}_I = \hbar g(\hat{\sigma}_+ + \hat{\sigma}_-)(\hat{a} + \hat{a}^\dagger). \tag{3.6.7}$$

Now equations (3.6.2),(3.6.3) and (3.6.7) are plugged into equation (3.6.1) to obtain the total Hamiltonian

$$\hat{H} = \underbrace{\hbar\omega\hat{a}^\dagger\hat{a}}_{\hat{H}_F} \underbrace{- \frac{1}{2}\hbar\omega_0\hat{\sigma}_z}_{\hat{H}_0} + \underbrace{\hbar g(\hat{\sigma}_+ + \hat{\sigma}_-)(\hat{a} + \hat{a}^\dagger)}_{\hat{H}_I}. \tag{3.6.8}$$

In order to simplify this expression further, we need to introduce the "interaction picture". In this picture, the eigenstates for the uncoupled Hamiltonian, including their time dependence, are choosen as basis for the state vectors. Note that this means that the only time dependence for the coefficients comes from the coupling which allows us to isolate the effect of the coupling from the behavior of the uncoupled system. One downside however, is that one also has to take into account that the operators are time dependent in this picture. See [8] for more information. In the interaction picture, the time evolution of the creation- and annihilation operators as well as the atomic transition operators are given by

$$\begin{aligned}\hat{a}(t) &= \hat{a}(0)e^{-i\omega t},\\ \hat{a}^\dagger(t) &= \hat{a}^\dagger(0)e^{i\omega t},\\ \hat{\sigma}_\pm(t) &= \hat{\sigma}_\pm(0)e^{\pm i\omega_0 t}.\end{aligned} \tag{3.6.9}$$

In carrying out the multiplication in the interaction part of the Hamiltonian in equation (3.6.8), there are four terms:

$$\begin{aligned}\hat{\sigma}_+\hat{a}(t) &\sim e^{i(\omega_0-\omega)t},\\ \hat{\sigma}_-\hat{a}(t)^\dagger &\sim e^{-i(\omega_0-\omega)t},\\ \hat{\sigma}_+\hat{a}(t)^\dagger &\sim e^{i(\omega_0+\omega)t},\\ \hat{\sigma}_-\hat{a}(t) &\sim e^{-i(\omega_0+\omega)t}.\end{aligned} \tag{3.6.10}$$

For a small detuning, i.e. $|\Delta| \ll \omega_0$,ω, it is valid to apply the RWA. This is the same method as in the Rabi model but here also note that $\hat{\sigma}_+\hat{a}(t)^\dagger$ describes the emission of a photon and an excitation of the qubit and the term $\hat{\sigma}_-\hat{a}(t)$ describes the absorption of a photon with the qubit going from the excited to the ground state. Both of these terms are non-energy conserving.

After the RWA is applied the remaining terms are

$$\hat{H} = \hbar\omega\hat{a}^\dagger\hat{a} - \frac{1}{2}\hbar\omega_0\hat{\sigma}_z + \hbar g(\hat{\sigma}_+\hat{a} + \hat{\sigma}_-\hat{a}^\dagger), \tag{3.6.11}$$

which is known as the Jaynes-Cummings Hamiltonian and describes the full system of the qubit coupled to a cavity resonator. The terms $\hat{\sigma}_+\hat{a}$ and $\hat{\sigma}_-\hat{a}^\dagger$ are the only ones that give rise to off diagonal elements in the Hamiltonian matrix. This is what causes the coupling of the energy levels in the system and a characteristic way this is seen is when energy levels avoid each other. This is commonly referred to as avoided level crossings and is an indicator for when coupled quantum states have been obtained.

When reading out the state of the qubit, the idea is to measure the resonance frequency of the cavity, which changes depending on the state of the qubit. Assuming that the qubit and cavity is a bit off resonance, such that $\omega, \omega_0 \gg |\Delta| \gg g$, and performing perturbation expansion in the parameter $\frac{g^2}{\Delta}$ on equation (3.6.11) gives

$$\hat{H}_{disp} = \hbar\left(\omega - \frac{g^2}{\Delta}\hat{\sigma}_z\right)\hat{a}^\dagger\hat{a} - \frac{\hbar}{2}\left(\omega_0 + \frac{g^2}{\Delta}\right)\hat{\sigma}_z. \tag{3.6.12}$$

This is known as the dispersive Jaynes-Cummings Hamiltonian and it is easy to see that the resonance frequancy depends on the qubit state from the terms with σ_z which have expectation values depending on the qubit state.

Looking at equation (3.6.11) it is interesting to examine the atomic inversion to see the differences between the Jaynes Cummings model and the Rabi model. Consider two different initial states for the cavity, first a number state, which is just the field constrained to have a certain number of photons and secondly a coherent state, which is the most "classical" quantum state because it behaves mostly like the wave interpretation of the EM field. Figure 5 shows the atomic inversion when the cavity resonator is in a number state and behaves like the atomic inversion within the Rabi model, compare to figure 3. This is a bit surprising because a number state is very "quantum", the field is quantized with only a few photons in the cavity resonator.

To the contrary, when the cavity resonator is put in a coherent state, the inversion behaves like in figure 6 which does not look at all like it did in the Rabi model, figure 3. As seen, the inversion amplitude is not constant but seems to die out and then revives. This shows that it is important to take the quantization of the field into account in order to get the correct description.

Another big difference between the Rabi model and the Jaynes-Cummings model is that JC model exhibits Rabi oscillations even when the field has zero photons, i.e. $\hat{n}|n\rangle = 0$. In the Rabi model there always has to be a field present in order to observe this phenomena.

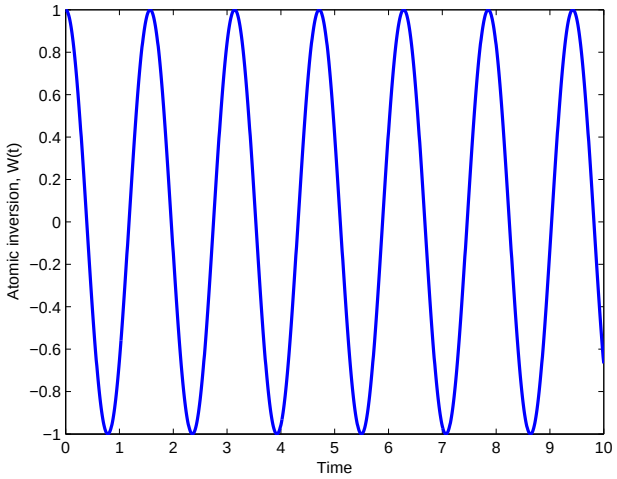

Figure 5: This is the atomic inversion when the cavity resonator is initially in a number state. As seen it behaves like in the semiclassical Rabi model (figure 3).

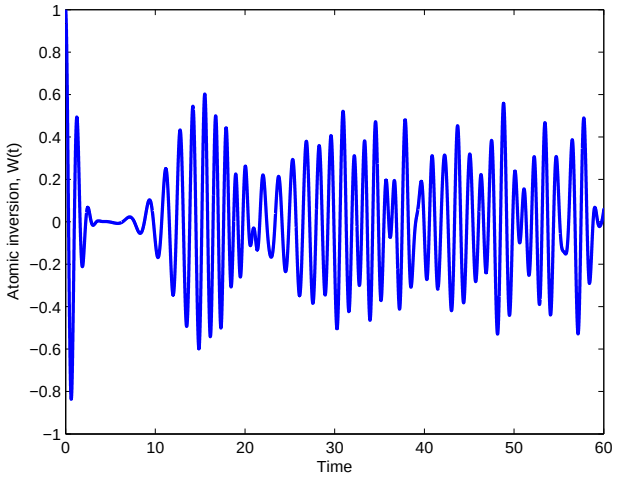

Figure 6: This is the atomic inversion when the cavity resonator is initially in a coherent state, where the expected number of photons are 5. This does not behave like in the Rabi model (figure 3) but it seems to die out around T=10 and then revives again.

4 Theory - Part II

The theory presented in the previous section is sufficient when the influence of environment is neglected. In this section, we introduce some additional concepts to be able to discuss decoherence.

First we introduce the density matrix, which is a general representation of quantum states. With the density matrix notation, we obtain an economic way of describing the influence of the surrounding environment. A general discussion of decoherence, noise and how to

read-out a qubit follows and completes the theory. We would like to point out that the density matrices as well as the theory of noise are important in the field of quantum computing. However, in our analysis we have not used them, so the theory section part II is not necessary to understand the data analysis in section 6.

4.1 The Density Matrix - Pure States and Mixed States

To describe decoherence, that is, how qubits are influenced by a noisy environment, three useful concepts are introduced; pure states, mixed states and density matrices. Quantum states described by state vectors are said to be pure states. Complete knowledge of not only the probability amplitudes but also the phase is needed to conclude that a state is a pure state. On the contrary, quantum states that cannot be described by state vectors are said to be mixed states. Previous undergraduate courses in quantum mechanics have only considered pure states.

To understand the difference between pure and mixed states an example with two ensembles follows. The term ensemble is used for a collection of several qubits. Consider a pure ensemble, e.g. where the qubits are in an equal superpositions of $|0\rangle$ and $|1\rangle$. The pure state

$$|\Psi_0\rangle = \frac{1}{\sqrt{2}}\left(|0\rangle + |1\rangle\right),$$

describes an element in such an ensemble. Then, consider also a mixed ensemble, with the probability $P_{0/1} = 0.5$ to be in either $|0\rangle$ or $|1\rangle$. A mixed ensemble has classical properties in the sense that it can be analogously thought of as flipping a coin and observe the outcome. The mixed ensemble we are considering looks like

$$\Big\{|0\rangle,\, |1\rangle,\, |1\rangle,\, \ldots\, ,\, |0\rangle,\, |1\rangle,\, |0\rangle\Big\},$$

where the ensemble contains many qubits, equally many in $|0\rangle$ and $|1\rangle$. If we pick one qubit from either of the ensembles and perform a measurement, to determine the state of the qubit, the measurement will give $P_{0/1} = 0.5$ independent of the originating ensemble. Therefore we try to distinguish the two ensembles by a rotation operation $R_z(\pi/2)$. After the rotation the superposed state $|\Psi_0\rangle$ evolves into $|0\rangle$ since

$$R_z(\pi/2)|\Psi_0(\pi/2{,}0)\rangle = |\Psi_0(0{,}0)\rangle = |0\rangle,$$

so a measurement give $|0\rangle$ with unit probability. Whereas a rotation on a qubit in the mixed ensemble, will evolve into equal superpositions. The ensemble will explicitly look like

$$\left\{\frac{1}{\sqrt{2}}(|0\rangle - |1\rangle), \frac{1}{\sqrt{2}}(|0\rangle + |1\rangle),\ \ldots\ , \frac{1}{\sqrt{2}}(|0\rangle - |1\rangle)\right\},$$

then a measurement after the rotation give $|0\rangle$ and $|1\rangle$ with equal probability $P_{0/1} = 0.5$. The conclusion is that the pure state and the mixed state are not equivalent and to describe this difference, the density operator and density matrix are introduced.

4.1.1 The Density Operator

The density operator $\hat{\rho}$ is defined as

$$\hat{\rho} = \sum_i p_i |\Psi_i\rangle\langle\Psi_i|,$$

where p_i is the probability to be in state $|\Psi_i\rangle$. Note that the density operator is independent of basis. To map the density operator for a qubit onto the density matrix, a basis for the two-level system has to be chosen. For a complete basis $|b_i\rangle$, the density matrix is defined to have the elements

$$\rho_{kl} = \sum_i p_i \langle b_k|\Psi_i\rangle\langle\Psi_i|b_l\rangle, \tag{4.1.1}$$

which forms a two-by-two matrix

$$\rho = \begin{bmatrix} \rho_{00} & \rho_{01} \\ \rho_{10} & \rho_{11} \end{bmatrix}.$$

The probability to find the qubit in a certain state is given by the diagonal elements $\rho_{00/11}$, whereas the off-diagonal elements, $\rho_{01/10}$, give the amount of coherence between the states.

The expectation value of an operator $\hat{O}$ with matrix elements $O_{kl} = \langle b_k|\hat{O}|b_l\rangle$ are calculated the following way

$$\begin{aligned}
\langle\hat{O}\rangle &= \sum_i p_i \langle\Psi_i|\hat{O}|\Psi_i\rangle \\
&= \sum_i p_i \langle\Psi_i| \left(\sum_k \sum_l |b_l\rangle\langle b_l|\hat{O}|b_k\rangle\langle b_k| \right) |\Psi_i\rangle \\
&= \sum_i p_i \sum_k \sum_l \langle\Psi_i|b_l\rangle\langle b_l|\hat{O}|b_k\rangle\langle b_k|\Psi_i\rangle \\
&= \sum_k \sum_l \left(\sum_i p_i \langle b_k|\Psi_i\rangle\langle\Psi_i|b_l\rangle \right) \langle b_l|\hat{O}|b_k\rangle \\
&= \sum_k \sum_l \rho_{kl} O_{lk} \\
&= \sum_k (\rho O)_{kk},
\end{aligned}$$

where the last expression is called the trace of $\rho\hat{O}$, which is denoted

$$\langle\hat{O}\rangle = Tr(\hat{\rho}\hat{O}) = Tr(\hat{O}\hat{\rho}), \tag{4.1.2}$$

where the last equality $Tr(\hat{\rho}\hat{O}) = Tr(\hat{O}\hat{\rho})$ follows from the symmetry of the summation in the calculation above. Furthermore, the density matrix is Hermitian, i.e. $\rho^\dagger = \rho \Leftrightarrow \rho_{kl} = \rho^*_{lk}$, which follows from the definition (4.1.1) and has trace unity, since

$$\begin{aligned}
Tr(\rho) &= \sum_i p_i \sum_k \langle b_k|\Psi_i\rangle\langle\Psi_i|b_k\rangle \\
&= \sum_i p_i \sum_k \langle\Psi_i|b_k\rangle\langle b_k|\Psi_i\rangle \\
&= \sum_i p_i \langle\Psi_i| \left(\sum_k |b_k\rangle\langle b_k| \right) |\Psi_i\rangle \\
&= \sum_i p_i \langle\Psi_i|\Psi_i\rangle = \sum_i p_i = 1.
\end{aligned} \tag{4.1.3}$$

A pure state can be written as a superposition $|\Psi\rangle$, with the corresponding density operator $\hat{\rho} = |\Psi\rangle\langle\Psi|$. For a pure state it is then clear that

$$\hat{\rho}^2 = |\Psi\rangle\langle\Psi|\Psi\rangle\langle\Psi| = |\Psi\rangle\langle\Psi| = \hat{\rho} \quad \Rightarrow \quad Tr(\hat{\rho}^2) = Tr(\hat{\rho}) = 1,$$

the trace of the squared density operator equals unity. For a mixed state, an arbitrary statistical mixture can be expressed as

$$\hat{\rho}^2 = \sum_j \sum_k p_j p_k |\Psi_j\rangle\langle\Psi_j|\Psi_k\rangle\langle\Psi_k|,$$

and the corresponding calculation of the trace

$$\begin{aligned}
Tr(\hat{\rho}^2) &= \sum_i \langle b_i|\hat{\rho}^2|b_i\rangle \\
&= \sum_i \langle b_i| \left(\sum_j \sum_k p_j p_k |\Psi_j\rangle\langle\Psi_j|\Psi_k\rangle\langle\Psi_k| \right) |b_i\rangle \\
&= \sum_j \sum_k p_j p_k \langle\Psi_j|\Psi_k\rangle \left(\sum_i \langle b_i|\Psi_j\rangle\langle\Psi_k|b_i\rangle \right) \\
&= \sum_j \sum_k p_j p_k \langle\Psi_j|\Psi_k\rangle \left(\sum_i \langle\Psi_k|b_i\rangle\langle b_i|\Psi_j\rangle \right) \\
&= \sum_j \sum_k p_j p_k \langle\Psi_j|\Psi_k\rangle \left(\langle\Psi_k| \left(\sum_i |b_i\rangle\langle b_i| \right) |\Psi_j\rangle \right) \\
&= \sum_j \sum_k p_j p_k |\langle\Psi_j|\Psi_k\rangle|^2 \\
&\leq \left(\sum_j p_j \right) \left(\sum_k p_k \right) = 1,
\end{aligned}$$

where the equality holds only if $|\langle\Psi_j|\Psi_k\rangle|^2 = 1$ for every pair of states $|\Psi_i\rangle$ and $|\Psi_j\rangle$. This is possible only if all the $|\Psi_i\rangle$ differ with only an overall phase factor, which can only be true for a pure state. The conclusion is, by taking the trace of the squared density matrix, it is possible to distinguish pure states from mixed states

$$Tr(\hat{\rho}^2) = 1 \quad \text{for a pure state,} \tag{4.1.4}$$

$$Tr(\hat{\rho}^2) < 1 \quad \text{for a mixed state.} \tag{4.1.5}$$

4.1.2 Time-evolution of the Density Matrix

The Schrödinger equation $i\hbar\partial_t|\Psi(t)\rangle = \hat{H}|\Psi(t)\rangle$ governs the evolution of the system. Keep in mind that $\hat{H}$ is Hermitian, i.e. $\hat{H}^\dagger = \hat{H}$. We make use of the Schrödinger equation and

its Hermitian conjugate to derive

$$\begin{aligned} i\hbar\partial_t\hat{\rho}(t) &= i\hbar\sum_k p_k\partial_t|\Psi_k(t)\rangle\langle\Psi_k(t)| \\ &= \sum_k p_k\Big[\Big(i\hbar\partial_t|\Psi_k(t)\rangle\Big)\langle\Psi_k(t)| + |\Psi_k(t)\rangle\Big(i\hbar\partial_t\langle\Psi_k(t)|\Big)\Big] \\ &= \sum_k p_k\Big[\hat{H}|\Psi_k(t)\rangle\langle\Psi_k(t)| - |\Psi_k(t)\rangle\langle\Psi_k(t)|\hat{H}\Big] \\ &= \hat{H}\hat{\rho} - \hat{\rho}\hat{H} \quad = \quad [\hat{H},\hat{\rho}], \end{aligned} \tag{4.1.6}$$

which is known as the Liouville equation. The time-evolution of the density matrix is used to derive the equations describing how noise influence the evolution of a quantum state. If we know the time-evolution operator $\hat{U}(t)$, such that $|\Psi(t)\rangle = \hat{U}(t)|\Psi(0)\rangle$ the impact on the density matrix is simply

$$\begin{aligned} \hat{\rho}(t) &= \sum_k p_k|\Psi_k(t)\rangle\langle\Psi_k(t)| \\ &= \sum_k p_k\hat{U}(t)|\Psi_k(0)\rangle\langle\Psi_k(0)|\hat{U}^\dagger(t) \\ &= \hat{U}(t)\hat{\rho}(0)\hat{U}^\dagger(t). \end{aligned}$$

4.1.3 The Bloch Sphere for Mixed States

Any Hermitian 2×2 matrix can be decomposed into a weighted sum of Pauli and identity matrices. The density matrix is Hermitian, hence it can be decomposed. An arbitrary single qubit density matrix can be expressed as

$$\rho = \frac{\mathbf{1} + \mathbf{r}\cdot\hat{\sigma}}{2} = \frac{\mathbf{1} + r_x\hat{\sigma}_x + r_y\hat{\sigma}_y + r_y\hat{\sigma}_y}{2} \qquad \text{with } |\mathbf{r}| \leq \mathbf{1},$$

where $\mathbf{r} = (r_x,r_y,r_z)$ is the the Bloch vector and $\hat{\sigma} = (\hat{\sigma}_x,\hat{\sigma}_y,\hat{\sigma}_z)$. Note that $Tr(\rho) = 1$, which is consistent with (4.1.3). From (3.2.2), the expectation values of Pauli matrices are projections of the qubit state onto the x, y and z-axis respectively. Using the trace formula (4.1.2) gives

$$\langle\hat{\sigma}_x\rangle = Tr(\rho\hat{\sigma}_x) = Tr\left(\frac{1}{2}\left[\mathbf{1}\hat{\sigma}_x + r_x\hat{\sigma}_x^2 + r_y\hat{\sigma}_y\hat{\sigma}_x + r_z\hat{\sigma}_z\hat{\sigma}_x\right]\right) = Tr\left(\frac{1}{2}r_x\mathbf{1}\right) = r_x,$$

using that $Tr(\hat{\sigma}_x) = Tr(\hat{\sigma}_y) = Tr(\hat{\sigma}_z) = 0$ and also that $Tr(\hat{\sigma}_i\hat{\sigma}_j) = 2\delta_{ij}$. Due to symmetry, we conclude that also $\langle\hat{\sigma}_y\rangle = r_y$ and $\langle\hat{\sigma}_z\rangle = r_z$. The length of the Bloch vector determines the state, a pure state is characterized by $|\mathbf{r}| = \mathbf{1}$ whereas for $|\mathbf{r}| < \mathbf{1}$ it is a mixed state. These requirements follow directly from (4.1.4), (4.1.5) and are easily verified by a calculation of the trace of the squared density matrix

$$\begin{aligned} Tr(\rho^2) &= Tr\left(\frac{1}{4}\left[\mathbf{1}^2 + 2(r_x\hat{\sigma}_x + r_y\hat{\sigma}_y + r_z\hat{\sigma}_z) + (r_x\hat{\sigma}_x + r_y\hat{\sigma}_y + r_z\hat{\sigma}_z)^2\right]\right) \\ &= Tr\left(\frac{1 + r_x^2 + r_y^2 + r_z^2}{4}\mathbf{1}\right) = \frac{1 + |\mathbf{r}|^2}{2}. \end{aligned}$$

The interpretation of $|\mathbf{r}|$, in order to visualize, is that pure states are on the surface of the sphere, whilst mixed states are inside.

4.1.4 Reduced Density Matrix of Composite Systems

A two qubit system is the smallest non-trivial composite system that could be used for analysis of interactions between qubits. The system can also be used to analyze the simplest coupling with the environment, i.e. where the environment is another qubit. Any pure two qubit state can be expressed as

$$|\Psi\rangle = c_{00}|0_1\rangle|0_2\rangle + c_{01}|0_1\rangle|1_2\rangle + c_{10}|1_1\rangle|0_2\rangle + c_{11}|1_1\rangle|1_2\rangle, \tag{4.1.7}$$

where the coefficients c_{ij} satisfy normalization. The expectation value of an operator $\hat{O} = \hat{O}_1 \otimes \hat{1}_2$ acting only on the first qubit is calculated as follows

$$\begin{aligned}\langle\Psi|\hat{O}|\Psi\rangle &= \Big[c_{00}^*\langle 0_1|\langle 0_2| + c_{01}^*\langle 0_1|\langle 1_2| + c_{10}^*\langle 1_1|\langle 0_2| + c_{11}^*\langle 1_1|\langle 1_2|\Big]\Big(\hat{O}_1 \otimes \hat{1}_2\Big) \\ &\quad \Big[c_{00}|0_1\rangle|0_2\rangle + c_{01}|0_1\rangle|1_2\rangle + c_{10}|1_1\rangle|0_2\rangle + c_{11}|1_1\rangle|1_2\rangle\Big].\end{aligned}$$

Performing the multiplication gives 16 terms, with only 8 distinct from zero, due to orthogonality. We regroup the remaining terms

$$\begin{aligned}\langle\Psi|\hat{O}|\Psi\rangle &= \langle 0_1|\hat{O}|0_1\rangle(|c_{00}|^2 + |c_{01}|^2) + \langle 0_1|\hat{O}|1_1\rangle(c_{00}^*c_{10} + c_{01}^*c_{11}) \\ &+ \langle 1_1|\hat{O}|0_1\rangle(c_{10}^*c_{00} + c_{11}^*c_{01}) + \langle 1_1|\hat{O}|1_1\rangle(|c_{10}|^2 + |c_{11}|^2),\end{aligned}$$

and thus, the second qubit is traced out. The construction of the reduced density matrix ρ_1 is straightforward

$$\rho_1 = \begin{bmatrix} |c_{00}|^2 + |c_{01}|^2 & c_{10}^*c_{00} + c_{11}^*c_{01} \\ c_{00}^*c_{10} + c_{01}^*c_{11} & |c_{10}|^2 + |c_{11}|^2 \end{bmatrix}. \tag{4.1.8}$$

It follows that ρ_1 is Hermitian, and normalization gives $Tr(\rho_1) = 1$, so the reduced density matrix is a valid density matrix. The extension of the reduced density matrix to consider more then one qubit is done analogous to the calculation above using the tensor product. As we will se in the next section, coupling to a noisy environment, causes the off-diagonal elements to decay. So, the environment tries to make the density matrix diagonal, in some basis. This effect is called decoherence and must be limited to perform quantum computing.

4.2 Decoherence

The main problem with constructing a quantum computer is decoherence. This is when the exact time evolution of the qubit cannot be controlled so that the qubit state will vary between different repetitions of the experiment. This means that the state of the qubit is unknown, which results in that the qubit will have a probability distribution to be in different states, i.e. a mixed state.

The physical explanation for decoherence is interaction with the environment, for example when the energy in the system is dissipated. This can be induced by impurities and defects in the materials or unwanted electromagnetic field interaction. Decoherence will gradually force superpositions into less coherent states, and the system evolves into unknown states.

In section 4.1 the density matrix was introduced as a way to describe a mixed state. Even though there are several mixed states that corresponds to one density matrix, it can

express all measurable information about the qubit state. This makes the density matrix ideal for describing decoherence.

The time evolution of the density matrix for a single qubit under the influence of noise can be derived by assuming that it is affected by a Hamiltonian

$$\hat{H} = -\frac{\hbar\omega_0}{2}\hat{\sigma}_z - \frac{\delta\mathbf{B}(t)}{2}\cdot\hat{\sigma} = -\frac{\hbar\omega_0}{2}\hat{\sigma}_z - \frac{1}{2}\left[\delta B_x, \delta B_y, \delta B_z\right]\left[\hat{\sigma}_x, \hat{\sigma}_y, \hat{\sigma}_z\right],$$

consisting of a constant energy spacing of $\hbar\omega_0$ and noise. The last term is expressing a scalar product of matrices. For a specific noise function $\delta\mathbf{B}(t)$, $\dot{\rho}$ can be expressed by the Liouville equation (4.1.6). In reality, the actual function for the noise is by all means unknown and the time evolution for the reduced density matrix of the qubit is given by averaging over the noise distribution, tracing out the noise. Using this, the time evolution of ρ can be expressed in terms of a noise field $\mathbf{S}(\omega)$, known as the spectral noise density.

The effects of decoherence can be divided into dephasing and mixing/relaxation. Mixing is when the probability to measure the qubit in the $|0\rangle$ or $|1\rangle$ state changes. In time this will make it impossible to determine which state the qubit originally was in. Since the two states have different energies, mixing implies that the qubit exchanges energy with the surroundings. If the temperature of the surroundings is low enough it will not have any energy to give to the qubit. Consequently, in time, the energy of the qubit will dissipate to the surroundings, which relaxes the qubit to the ground state. This phenomenon is called relaxation and in reality it is used to initialize the qubit in the ground state.

Treating the environment quantum mechanically, i.e. placing the qubit in a bath of harmonic oscillators at thermal equilibrium with temperature T [3], the time-evolution of the density matrix due to mixing/relaxation is

$$\dot{\rho}_{00}(t) = -\Gamma_{\downarrow}\rho_{00}(t) + \Gamma_{\uparrow}\rho_{11}(t), \tag{4.2.1a}$$
$$\dot{\rho}_{11}(t) = \Gamma_{\uparrow}\rho_{00}(t) - \Gamma_{\downarrow}\rho_{11}(t). \tag{4.2.1b}$$

The excitation $\Gamma_{\uparrow}$ and relaxation $\Gamma_{\downarrow}$ rates of the qubit depend on the spectral noise density $\mathbf{S}(\omega)$, around frequencies for qubit transition $\omega = \pm\omega_0$. Their ratio is given by the Boltzmann distribution $\Gamma_{\uparrow}/\Gamma_{\downarrow} = e^{-\hbar\omega_0/k_BT}$, where $\hbar\omega_0$ is the energy spacing between $|0\rangle$ and $|1\rangle$. The diagonal terms will tend towards some distribution determined by the temperature T of the system with the characteristic time scale

$$\frac{1}{T_1} = \Gamma_{\downarrow} + \Gamma\uparrow,$$

which is called mixing time.

Dephasing comes from an uncertainty in the energy spacing for the qubit. In time, this will make the qubit lose all its phase information. In the density matrix the phase information is coded in the off-diagonal elements. When the qubit is affected by dephasing these will decrease exponentially with the characteristic time scale T_2, which is called dephasing time. T_2 can be decomposed into pure dephasing and dephasing induced by mixing/relaxation

$$\frac{1}{T_2} = \frac{1}{T_2^*} + \frac{1}{2T_1},$$

where $1/T_2^* \propto \mathbf{S}(\omega \approx 0)$ is the rate for pure dephasing and is caused by low frequency noise. Consequently, considering both dephasing induced by mixing and pure dephasing, the time evolution of the off-diagonal elements can be expressed as

$$\dot{\rho}_{01}^{rf}(t) = -\frac{1}{T_2}\rho_{01}^{rf}(t), \tag{4.2.2a}$$

$$\dot{\rho}_{10}^{rf}(t) = -\frac{1}{T_2}\rho_{10}^{rf}(t), \tag{4.2.2b}$$

which describes the total effect of dephasing. After sufficiently long time the off-diagonal elements will vanish and thus dephasing acts to make the density matrix diagonal. The index rf denotes the rotating frame where the considered system is precessing around the z-axis in the Bloch with constant velocity, see section 3.2.

A more compact way to describe the time evolution of a single qubit is the Bloch equations:

$$\dot{\mathbf{r}} = -\frac{1}{\hbar}\mathbf{B} \times \mathbf{r} - \frac{1}{T_1}(r_z - r_z^0)\hat{\mathbf{z}} - \frac{1}{T_2}(r_x\hat{\mathbf{x}} + r_y\hat{\mathbf{y}}). \tag{4.2.3}$$

Here, r_z^0 denotes the steady state, when the qubit is in equilibrium with the environment and is determined by

$$r_z^0 = \frac{\Gamma_\downarrow - \Gamma_\uparrow}{\Gamma_\downarrow + \Gamma_\uparrow} = \tanh\frac{\hbar\omega_0}{2k_BT}.$$

The Bloch equations describe the motion of the vector on the Bloch sphere corresponding to the qubit state. In this picture, the qubit is affected by a constant magnetic field $\mathbf{B}$. Dephasing will act to decrease the x and y components of the vector and thus project the vector on the z axis while relaxation/mixing will make the z component converge towards r_z^0.

Note that (4.2.3) was referred to as the Bloch equations and not the Bloch equation. This is not a misprint, but rather a confusing convention. The plural refers to the $\hat{\mathbf{x}}$, $\hat{\mathbf{y}}$ and $\hat{\mathbf{z}}$ components of the equation.

4.3 Reading Out a Quantum Bit

Unless an experiment is set up in such a way before the measurement that the only states the qubit can end up in are $|0\rangle$ or $|1\rangle$, only one measurement will not suffice to determine the original state. The solution is to repeat the experiment and estimate the population, i.e. the ratio of $|0\rangle$ and $|1\rangle$. Other information of the state than the population may be obtained by performing operations on the qubit, turning other states into $|0\rangle$ and $|1\rangle$.

4.3.1 Back-action

In order to measure the qubit, it needs to be coupled to a detector. Besides the fact that this will open a channel for the qubit to be affected by the environment, which will lead to decoherence, an intrinsic property of the measurement process itself is that it will dephase the qubit.

Let the qubit initially be in the state $\alpha|0\rangle + \beta|1\rangle$ and the detector in its initial state $|e_i\rangle$. This gives their combined initial state as

$$|\Psi(t_0)\rangle = (\alpha|0\rangle + \beta|1\rangle)|e_i\rangle.$$

As the qubit and the detector become coupled, the detector should evolve into different states depending on the state of the qubit

$$|\Psi(t)\rangle = \alpha|0\rangle|e_0(t)\rangle + \beta|1\rangle|e_1(t)\rangle.$$

Now, considering the reduced density matrix for the qubit, tracing out the detector yields

$$\begin{aligned}
\rho_{red} &= Tr_{det}\Big((\alpha|0\rangle|e_0(t)\rangle + \beta|1\rangle|e_1(t)\rangle)(\alpha^*\langle 0|\langle e_0(t)| + \beta^*\langle 1|\langle e_1(t)|)\Big) \\
&= \alpha\alpha^* Tr\left(|e_0(t)\rangle\langle e_0(t)|\right)|0\rangle\langle 0| + \alpha\beta^* Tr\left(|e_0(t)\rangle\langle e_1(t)|\right)|0\rangle\langle 1| \\
&\quad + \alpha^*\beta Tr\left(|e_1(t)\rangle\langle e_0(t)|\right)|1\rangle\langle 0| + \beta\beta^* Tr\left(|e_1(t)\rangle\langle e_1(t)|\right)|1\rangle\langle 1| \\
&= |\alpha|^2\langle e_0(t)|e_0(t)\rangle|0\rangle\langle 0| + \alpha\beta^*\langle e_1(t)|e_0(t)\rangle|0\rangle\langle 1| + \alpha^*\beta\langle e_0(t)|e_1(t)\rangle|1\rangle\langle 0| \\
&\quad + |\beta|^2\langle e_1(t)|e_1(t)\rangle|1\rangle\langle 1| \\
&= \begin{pmatrix} |\alpha|^2 & \alpha\beta^*\langle e_1(t)|e_0(t)\rangle \\ \alpha^*\beta\langle e_0(t)|e_1(t)\rangle & |\beta|^2 \end{pmatrix}.
\end{aligned}$$

So both the off-diagonal elements depend on $\langle e_0|e_1\rangle$. To be able to distinguish two quantum states they need to be orthogonal. Thus, for the detector to work, the states $|e_0(t)\rangle$ and $|e_1(t)\rangle$ needs to evolve into two orthogonal states which means that the off-diagonal components of ρ_{red} tends to zero and the system becomes dephased.

This measurement-induced dephasing can be expressed by a dephasing rate Γ_φ. Denoting the time needed to measure the qubit as t_{ms}, the quantum efficiency for the measurement can be defined as $\eta = (t_{ms}\Gamma_\varphi)^{-1}$. This is interesting to consider as a benchmark of the measurement process. For an ideal measurement the quantum efficiency is 1, however if the measurement induces additional dephasing the quantum efficiency will be lower.

The derivation above assumes that the detector does not change the population of the qubit. A measurement process that has this property is called Quantum Nondemolition (QND). For not perfect QND processes the measurement can induce mixing, i.e. change in population, which means that $|\alpha|^2$ and $|\beta|^2$ are affected. This mesurement induced mixing, is characterized by a time scale T_1. To obtain a quality factor of the signal, we define the signal to noise ratio as

$$\text{SNR} = \frac{T_1}{t_{ms}},$$

which for a good readout should be $\gg 1$.

4.3.2 Read-Out in Circuit Cavity

The exact read-out process differs between different realizations of qubits. For the transmon qubit coupled to a cavity resonator the cavity frequency will shift a bit depending on the qubit state. This can be seen in the dispersive Jaynes-Cummings Hamiltonian (3.6.12), where the resonance frequency of the cavity is given by

$$\omega_{eff} = \omega - \frac{g^2}{\Delta}\sigma_z = \omega \pm \frac{g^2}{\Delta}, \tag{4.3.1}$$

where minus corresponds to a qubit in ground state and plus to the excited state. So, if the qubit is in the excited state, the cavity resonance frequency will be slightly changed. This dependence, between the qubit state and cavity resonance frequency, makes the readout of a transmon fairly uncomplicated.

The cavity resonance frequency can be determined by sending microwaves into the cavity with a frequency corresponding to one of these resonance frequencies. On resonance, the probability for the photons in the incoming signal to be absorbed by the cavity (instead of reflected) is higher and thus it is expected to see a decrease in the reflection coefficient at this frequency. After enough photons are sent into the cavity the difference in amount of reflected photons depending on the qubit state will be statistically significant.

Seen from the point of view of the qubit, there will be an uncertainty in the energy difference between the qubit states due to uncertainty in the number of photons, that has been in the cavity. This will gradually dephase the qubit.

5 Qubit Realization

There are many different ideas how to construct qubits. One proposal is to use real atoms or molecules to store information as nucleus spin or electronic states. Another promising qubit type is the superconducting qubit.

So far, trapped ion qubits are the qubit type where quantum computing have been most successful. In 1995, Cirac and Zoller presented a way of making qubits out of ions [15]. The ions are trapped by an electromagnetic field in a vacuum chamber. Lowering the temperture, information can be stored as electronic states in each ion and operated by interaction through Coulomb forces between the ions. In 2009, researchers at University of Innsbruck [16] demonstrated a realization of quantum computation with "decoherence free" ion trap qubits [17]. Note that they still have decoherence in the experiment but they have achieved a great improvement.

Another successful qubit type is NMR, Nuclear Magnetic Resonance, which is a well known technique among other applications for determine the structure in compounds. In NMR it is the spins of atomic nuclei which are serving as qubits. Unlike the trapped ion qubit the NMR qubit is not a single atom but an ensemble of molecules. Operations are performed by applying magnetic field pulses. This affects the spins coupled by chemical bonds between atoms. In 2001, a successful implementation of Shor's algorithm to factorize the number 15 was made using NMR qubits [18].

Trapped ions and NMR are examles of atomic qubit realizations and are both successful methods to perform operations. Because of the difficulties in building multi-qubit systems with atomic qubits another qubit type is suggested, the superconducting qubit.

Superconducting qubits are nanometer-scale superconducting circuits working as artifical atoms with engineered energy levels. All these superconducting qubits are based on Josephson junctions, as will be discussed in section 5.1. The "atoms" can be manipulated by currents, voltages and microwave photons, which can be used to control the tunneling of Cooper pairs in the Josephson junctions. Examples of such qubits in addition to the transmon are charge (figure 10a), phase (figure 10b) and flux qubits. Building a system of many superconducting qubits, the problem is not the coupling between them, as in atomic qubit types, but minimizing the coupling to the environment.

The primary problem for all types of qubit realizations is that very few operations can be performed before the qubit looses its quantum coherence. While the trapped ion qubit has exhibited relatively long coherence time it is limited by the weak coupling between the qubits. Operations on qubits, controlling and measuring, requires a good coupling to the environment. The desired environment includes control and measurement instruments, but the surroundings also contain noise sources. Consequently coupling is needed but inevitably leads to decoherence.

An advantage of artifical atoms is that they are more tunable than other systems [19]. Even though they have strong coupling they exhibit good coherence. They also have the advantage that they are easy to fabricate, as fabricating small chips is a well-established technique and a process possible to scale up.

5.1 Josephson Junction

To understand the realization of a superconducting qubit, we need to explain superconductivity and the Josephson junction. Superconductivity is a phase transition where paired electrons (Cooper pairs) causes the electrical current to flow through the conductor without any dissipation. The Josephson junction is a non-linear electrical component using superconductivity. Because of the low dissipation in superconductors quantum phenomena become observable.

Superconductivity was first observed in 1911 and is characterized by a sudden disappearance of electrical resistivity which occurs at a temperature specific to the material. Briefly, electrical resistance is caused by electrons colliding with impurities and other defects in the material and energy dissipation occurs. Under a critical temperature, depending on the material, the electrons are forced into bound pairs (Cooper Pairs) and establish a coupling energy. In order to scatter an individual electron the Cooper pair would need to be broken and to break the pair, the energy in the system has to be larger than the coupling energy. Simply said, the Cooper pairs avoid scattering, which causes the resistivity to drop to zero [20].

Superconducting qubits consist of standard components such as capacitors, inductors and also Josephson junctions. It is possible to quantize the circuit [21] by setting up the Lagrange equations (the equations of motion in Lagrangian mechanics [22]) and introducing, as in section 3.5, canonical variables and imposing quantum commutation rules. From the Lagrange equations the Hamiltonian can be derived expressing the total energy of the system. However, this analysis is beyond the scope of this report.

The reason for introducing the Josephson junction is that electrical circuits based solely on capacitors and inductors are linear resonators, which are quantized to quantum harmonic oscillators. This obstructs the desired isolation of two energy states as all energy states are equidistant with separation $\hbar\omega$ (figure 7). When excitations occur, the system is easily excited to higher levels than the first excited state. To make the circuit a suitable two level system we need to modify it and introduce a non-linearity, created by the Josephson junction, which will make the energy spacing non-equidistant, i.e. introduce anharmonicity. Thus the ground state $|0\rangle$ and and the first excited state $|1\rangle$ can be isolated and therefore used to represent a qubit.

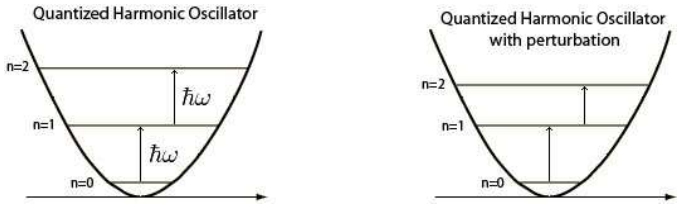

Figure 7: To the left: the quantized harmonic oscillator. To the right: the desired modification where the transition energy between $|0\rangle \rightarrow |1\rangle$ differs from $|1\rangle \rightarrow |2\rangle$. By using, for example, photons with angular frequency ω on resonance with energy difference $E_1 - E_0$, the dynamics can be limited to these two levels, E_0 corresponding to the ground state $|0\rangle$ and E_1 to the first excited state $|1\rangle$.

The Josephson Junction consists essentially of two superconducting plates separated by a thin isolating barrier, see figure 8. Basically, Cooper Pairs in the superconductors are

tunneling through the junction, and causes the current to have a non-linear dependence on the phase difference across the junction. This in turn gives rise to the desired anharmonicity in the system. The current and the voltage across the Josephson junction are described by the two Josephson equations [23]. The first (5.1.1) represents the dissipationless current I through the junction, which is also known as the DC Josephson effect:

$$I = I_C \sin(\varphi), \tag{5.1.1}$$

where $\varphi = \theta_2 - \theta_1$ is the phase difference between the wave functions in each superconductor. I_C is the critical Josephson current, i.e. the maximum dissipationless current that the junction supports. The second equation (5.1.2), is a relation between the time derivative of φ and the voltage drop V, across the junction

$$\frac{d\varphi}{dt} = \frac{2\pi}{\Phi_0} V, \tag{5.1.2}$$

where $\Phi_0 = \frac{h}{2e}$ is the flux quantum. This equation is called the AC Josephson effect. The energy stored in the Josephson junction is obtained by the integral (using (5.1.1) and (5.1.2)),

$$\int_{-\infty}^{t} I(\tau)V(\tau)\mathrm{d}\tau = \frac{\hbar I_C}{2e}\int_{-\infty}^{t} \sin(\varphi(\tau))\dot{\varphi}(\tau)\mathrm{d}\tau = -E_J \cos(\varphi(t)), \tag{5.1.3}$$

where $E_J = \hbar I_C/2e$. The right hand side in this equation is called the Josephson energy. It is frequently used in Hamiltonians when describing the dynamics of the Josephson junctions.

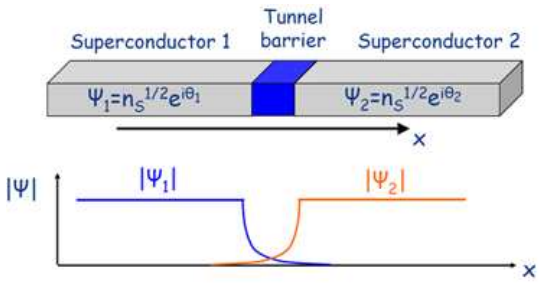

Figure 8: A Josephson junction. The wave functions describing each condensate overlap and hence tunneling is enabled. Courtesy of [3].

When adding a Josephson junction parallel to another, a superconducting loop can be created. Below, we show that the two Josephson junction can be regarded as one Josephson junction with a tuneable Josephson energy, depending on the magnetic flux penetrating the loop. This tunable loop is also called a superconducting quantum interference device (SQUID), see figure 9.

The two junctions give the resulting current

$$I = I_{c1}\sin(\varphi_1) + I_{c2}\sin(\varphi_2),$$

where I_{c1} and I_{c2} are the critical currents for each Josephson junction. Defining the terms

$$\varphi_d = \frac{\varphi_1 - \varphi_2}{2},$$

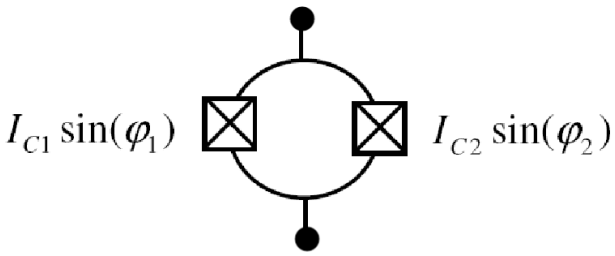

Figure 9: A circuit diagram of a SQUID where the magnetic field penetrates the loop, enclosed by the two Josephson Junction.

and

$$\varphi_s = \frac{\varphi_1 + \varphi_2}{2},$$

the current can be rewritten as

$$\begin{aligned} I = I_{c1}\left[\sin(\varphi_s)\cos(\varphi_d) + \sin(\varphi_d)\cos(\varphi_s)\right] + \\ + I_{c2}\left[\sin(\varphi_s)\cos(\varphi_d) - \sin(\varphi_d)\cos(\varphi_s)\right] = \\ = (I_{c1} - I_{c2})\sin(\varphi_d)\cos(\varphi_s) + (I_{c1} + I_{c2})\sin(\varphi_s)\cos(\varphi_d). \end{aligned}$$

Considering two identical junctions, i.e. $I_c = I_{c1} = I_{c2}$, this is reduced to

$$I = 2I_c \sin(\varphi_s)\cos(\varphi_d).$$

According to Tinkham [24], in the presence of a magnetic field Φ_{ext} the phase over a Josephson junction, can be replaced by a gauge-invariant phase leading to

$$\cos\varphi_d = \pm\cos\frac{\pi\Phi_{ext}}{\Phi_0}.$$

If defining a positive critical current

$$I_{cs} = 2I_c\left|\cos\left(\frac{\pi\Phi_{ext}}{\Phi_0}\right)\right|,$$

the SQUID can be viewed as a Josephson junction with an equivalent phase, φ_s, and a critical current tunable by an external magnetic field. Then the current through the SQUID is

$$I = I_{cs}(\Phi_{ext})\sin(\varphi_s).$$

As in calculating the energy for the single Josephson junction (5.1.3), the energy in the SQUID can be expressed in similar manner

$$E_S = \int_{-\infty}^{t} 2I_c\left|\cos\left(\frac{\pi\Phi_{ext}}{\Phi_0}\right)\right|\sin(\varphi_s)V(\tau)\mathrm{d}\tau = -\underbrace{E_{J0}\left|\cos\left(\frac{\pi\Phi_{ext}}{\Phi_0}\right)\right|}_{E_J(\Phi_{ext})}\cos\varphi_s. \qquad (5.1.4)$$

Here $E_J(\Phi_{ext})$ can be seen as the effective Josephson energy of the SQUID, and is tunable by the external magnetic field.

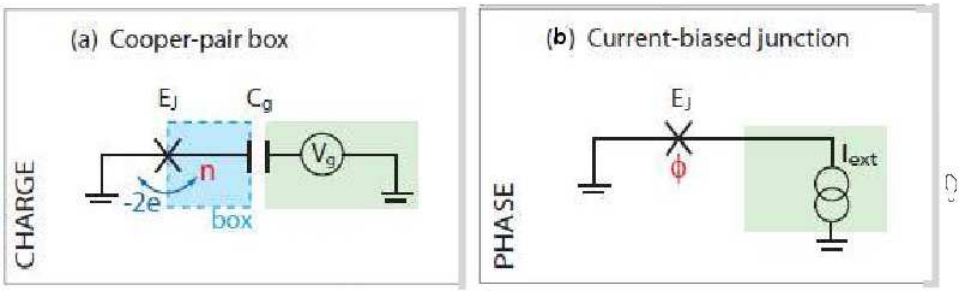

Figure 10: A schematic representation of two superconducting qubits, charge and phase. As seen, the charge qubit consists of a box connected via a Josephson junction to a reservoir to the left and via a gate capacitance to a gate voltage to the right. The phase qubit consists of a current source connected to a SQUID tunable by the magnetic field ϕ. Courtesy of [19].

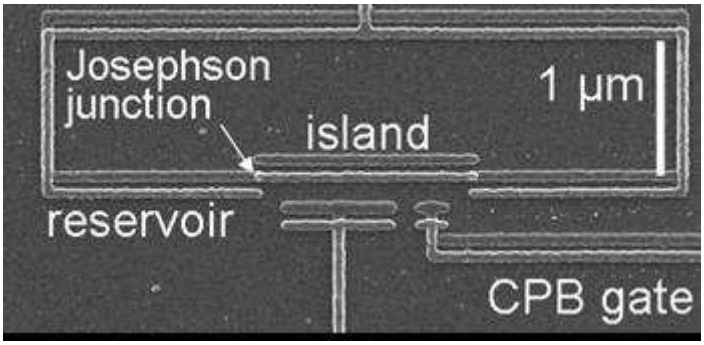

Figure 11: A SEM microscopy picture of a Cooper pair box circuit. As seen the island is connected to the rest of the circuit via two Josephson junctions, a superconducting loop also called a SQUID [25].

5.2 Charge Qubit

The first charge qubit was introduced by Nakamura et al. 1998 [4]. They showed that a superconducting island coupled via a Josephson junction to a reservoir could serve as a two-level system. This two-level system recieved the name Cooper pair box (CPB). Figure 11 shows a SEM microscopy picture of a Cooper pair box.

Figure 10a shows a circuit diagram of the CPB. The superconducting island (the box) is coupled to a gate via a capacitance C_g. Controlling the voltage over the gate the number of Cooper pairs on the island at equilibrium can be set. The qubit state is determined by the island charge, i.e. the number of Cooper pairs on the island. However, since the system consists of a large number of electrons the state is determined as the number of *extra* Cooper pairs tunneling on and off the island.

The Cooper pairs are induced on the island by the gate voltage as $n_g = \frac{C_g V_g}{2e}$, where C_g is the gate capacitance. n_g refers to the charge induced by the gate on the island, in units of Cooper pairs. To limit the system to two possible states, the gate voltage is controlled so that n_g only takes values between zero and one, i.e. there are either zero or one extra Cooper pair.

A single electron in the circuit contributes with a charging energy of $E_C \approx \frac{e^2}{2C_J}$, where

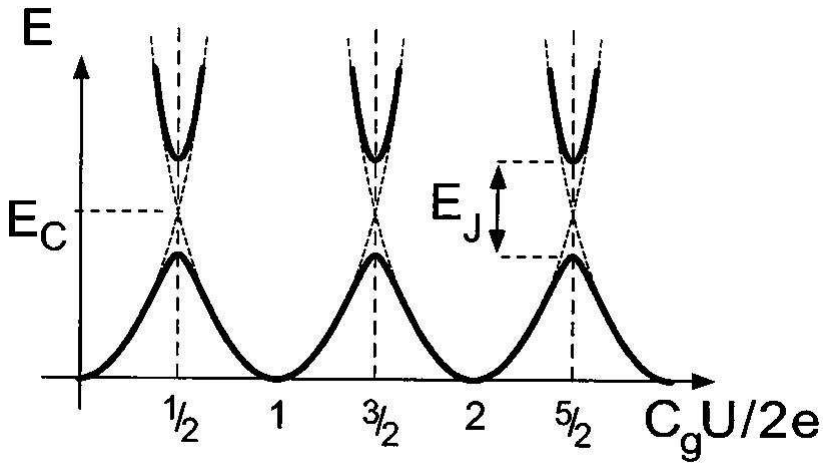

Figure 12: An energy diagram of the single Cooper pair box [26]. The x-axis represents n_g and the y-axis energy. At n_g equal to half integers avoided level crossings are seen. These points are also called degeneracy points for the CPB.

C_J is the capacitance of the junction. The charge qubit operates in the regime where the Josephson energy is much smaller than the charging energy, $E_J \ll E_C$. This means that the system has a well-defined charge but the phase is uncertain [27]. We thus describe the dynamics of the CPB in the charge basis $|n\rangle$, where n denotes the number of extra Cooper pairs on the island.

The Cooper pair box Hamiltonian consists of two terms, where the first term represents the energy added when an extra Cooper pair tunnels to the island and the second term is energy from the SQUID rewritten from (5.1.4) [6],

$$\hat{H} = 4E_C(\hat{n} - n_g)^2 - E_J \sum_{n=-\infty}^{\infty} \frac{1}{2} \left(|n\rangle\langle n+1| + |n+1\rangle\langle n| \right), \tag{5.2.1}$$

here $\hat{n}$ denotes the number operator in the charge basis $\hat{n}|n\rangle = n|n\rangle$. A method to calculate the eigenenergies of the CPB Hamiltonian (equation (5.2.1)) analytically is to use Mathieu functions [21]. Generally, Mathieu functions can be used in problems with resonance in forced oscillations.

In figure 12, the energy spectrum for the CPB can be seen. Note that the two energy lines avoid each other at n_g = half integers. These points are called degeneracy points and descend from the Josephson coupling. The dashed lines in the background indicate the case when $E_J = 0$ and in that case the energy levels would cross. At the degeneracy points the eigenstates of the system are equal superpositions of the neighbouring charge states.

5.3 Phase Qubit

In comparison to the charge qubit, the phase qubit is operated in the phase regime, i.e. at a very small charging energy and stronger Josephson coupling, $E_J \gg E_C$. Thus it

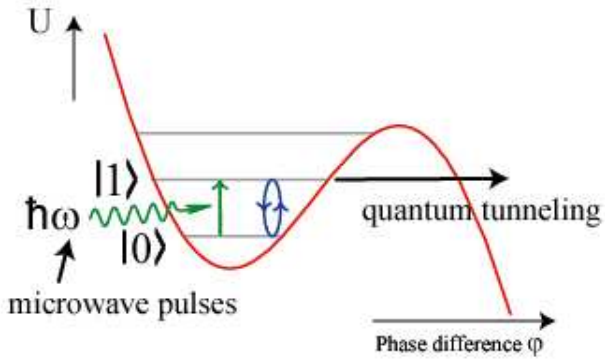

Figure 13: An energy diagram showing the potential the phase particle lives in and the energy levels in the potential well [30].

becomes insensitive to charge noise. However, it still is sensitive to magnetic flux, which makes it tunable [28].

To distinguish the phase qubit from the other superconducting qubits, it should be noticed that in the phase qubit the information is stored as phase differences across the Josephson junction [29]. One advantage of the phase qubit compared to the charge and the flux qubit is that its magnetic and electronic coupling to the environment is weak.

A phase qubit consists of a Josephson junction driven by a constant bias current, see figure 10b. The phase over the Josephson junction can be seen as a fictitious particle oscillating in a washboard potential, see figure 13. Affected by the bias current the potential tilts and for a bias current near I_C the phase particle can only exist in a few quantized states. By increasing the bias current even more tunneling effects appears in the potential and with some probability the particle can tunnel through the potential barrier, which can be measured as a voltage across the Josephson junction. Since the probability to tunnel is larger for the excited state than for the ground state, this technique can be used to determine the state of the qubit.

5.4 Transmon Qubit

The concept of the transmon qubit was first published in 2007 [6] and today both single and two-qubit operations have been performed. It is a qubit design derived from the Cooper pair box. However, instead of a single island coupled to a reservoir, the transmon consists of two superconducting islands coupled through two Josephson junctions isolated from the rest of the circuit. Another difference is that the transmon operates at a higher ratio between Josephson energy and charging energy. Considering also flux and phase qubits, the E_J over E_C ratio for the transmon is higher than the flux but lower than the one for the phase qubit. $\frac{E_J}{E_C}$ is for the transmon between 10^1 and 10^6. The increase in this ratio, as compared to the CPB, leads to a considerable reduction in charge noise sensitivity, while anharmonicity reduces more slowly and the energy spacing can be kept non equidistant. Less charge noise leads to smaller influence of gate charge fluctuations. Despite this modification, the transmon maintains the CPB insensitivity to other noise sources, like flux and critical current noise [6].

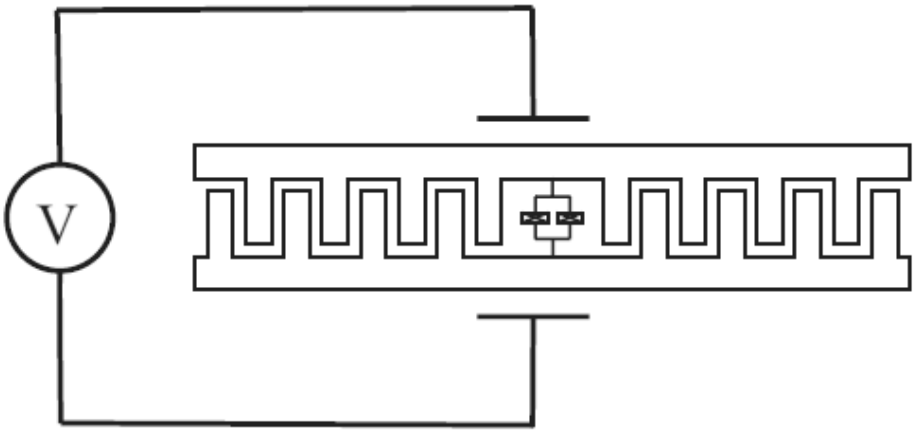

Figure 14: A transmon qubit capacitively coupled to the voltage source representing a cavity resonator. To the left the voltage source and to the right the transmon consisting of two Josephson junctions in a SQUID surrounded by superconducting metal islands. As can be seen, the islands are shaped as a large interdigitated ("finger") capacitor. Courtesy of [21].

The two Josephson junctions in the transmon forms a SQUID which makes the Josephson energy tunable, as in equation (5.1.4), by applying an external magnetic flux. To be able to perform measurements, the qubit is put into a cavity resonator. Photons can be sent into this cavity resonator to measure the combined frequency of the system, qubit and cavity resonator, which makes it possible to determine the state of the qubit.

The effective Hamiltonian of the transmon is the same as the one for the Cooper pair box, equation (5.2.1). The essential difference between the CPB and the transmon is the capacitor coupled as a shunting connection to the SQUID [6]. The capacitance is formed as two large superconducting islands, as can be seen in figure 14. This causes a reduction in E_C which in turn gives a higher $\frac{E_J}{E_C}$.

Extended from the CPB, the transmon Hamiltonian looks like [6]

$$\hat{H} = \underbrace{4E_C(\hat{n}-n_g)^2 - E_J \sum_{n=-\infty}^{\infty} \frac{1}{2}\Big(|n\rangle\langle n+1| + |n+1\rangle\langle n|\Big)}_{\text{CPB part}} + \underbrace{\hbar\omega_r \hat{a}^\dagger \hat{a}}_{\text{Field part}} + \underbrace{2\beta e V_{rms}^0 \hat{n}(\hat{a}+\hat{a}^\dagger)}_{\text{Interaction part}}. \tag{5.4.1}$$

This can be compared to the Jaynes-Cummings Hamiltonian, equation (3.6.11), they both consist of three parts, a qubit, field and interaction part. In the transmon Hamiltonian the first two terms are the qubit energy, the third term is the field energy identical to the Jaynes-Cummings field dependence and the last term describes the interaction between the field and the qubit. Here the Hamiltonian is written in the charge basis, it can also be expressed in the phase basis. In the charge basis, the state $|n\rangle$ corresponds to n Cooper pairs that have tunneled through the junction. ω_r represents the resonance frequency of the cavity resonator. β is a ratio between the gate capacitance and the total capacitance over the transmon. V_{rms}^0 comes from the coupling between the transmon and the cavity resonator. The notation implies that it is a root-mean-square value of the voltage, corresponding to a single photon in the cavity.

The eigenenergies for the transmon Hamiltonian, equation (5.4.1), can be approximated in the $E_C \ll E_J$ limit as [6]

$$E_m = -E_J + \sqrt{8E_J E_C}\left(m + \frac{1}{2}\right) - \frac{E_C}{12}(6m^2 + 6m + 3), \tag{5.4.2}$$

where $m = 0, 1, 2,....$ This implies that the transition energy between the zero and the one state can be calculated as

$$E_1 - E_0 = \sqrt{8E_J E_C} - E_C.$$

The transmon is a promising candidate as a qubit scalable up to the level of a usable quantum computer. According to Johansson (2009) [27] so far the transmon is the superconducting qubit with the longest coherence time demonstrated.

5.5 Fabrication

Fabrication of all superconducting qubits are performed in the same way. These qubits are metallic conductors placed on small chips called substrates. The substrate is often made of silicon, which is a bad conductor, and at low temperatures even an insulator. The metal can vary, but aluminium is often used. In order to produce superconducting circuits with nanometer precision, the qubits have to be fabricated in cleanrooms.

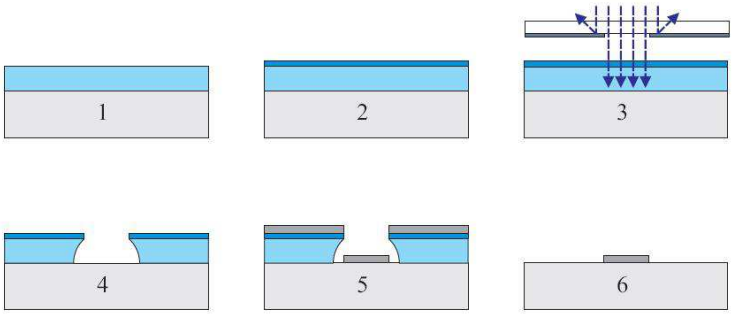

Figure 15: (1) First we see the substrate with one layer of photoresist. (2) A second resistive layer is sprayed on the photoresist. (3) The resist is exposed through a master mask. (4) The resist pattern is developed. (5) Next shows the conductor on the substrate and photoresist deposited. (6) To finish the process, the photoresist is removed and we have a conductor. Courtesy of [21].

First the chip is covered in a polymer called photoresist (figure 15.1, figure 15.2). To mark where the conductor should be placed, a mask is made (figure 15.3). The mask is a map with openings where the conductors are supposed to be. Then the mask is put on the substrate the photoresist is exposed to UV light (figure 15.4). UV light create marks in the resist where the conductors will be placed. Afterwards, metal is deposited (figure 15.5) and the photoresist is removed revealing a metal conductor (figure 15.6).

The smaller structures on the chip is made with electron beam lithography. In electron beam lithography a pattern can be directly written in the photoresist on the substrate. The stream of electrons is accelerated in an electric field and focused with magnetic lenses.

To achieve tunneling between two conductors, the metal is allowed to oxidize before the depositing a second layer. This forms a structure with two metal electrodes separated by a thin insulating barrier. Tunneling can occur between the two conductors through the metal oxide.

6 Data Analysis and Implementations

The experimental data we analyzed were obtained from microwave spectroscopy of a transmon placed in a cavity resonator. In figure 16 and figure 17 the data is presented. From now on we refer to figure 16 as dataset 1 and figure 17 as dataset 2. In the experiment that generated dataset 1, the transmon was tuned, whereas in dataset 2 the resonator was tuned. The tuning is accomplished by varying the magnetic flux through the SQUIDs. Since there are two SQUIDs in the circuit, one in the transmon and another one in the end of the cavity to terminate the resonator, it is possible to tune the qubit and the cavity resonator independently. By changing the magnetic flux through the terminating SQUID, the effective length of the cavity can be tuned. Changing the effective length, the length seen by photons in the cavity, implies tuning the resonance frequency.

The experiments were performed in a low temperature lab in MC2, with the circuit placed in a cryostat, which in short is a freezer able to operate in the mK range. The equipment is put in a cryostat for two reasons: to reach the superconducting temperature regime and to reduce effects of thermal noise. The measurement is performed by connecting a coaxial cable to the cavity, sweeping a suitable frequency range ($\sim$4-6GHz) and recording the reflection coefficient Γ of the system. When there is a frequency match between the applied field and the transition energies of the system, the energy radiated into the circuit will be absorbed and the magnitude of the reflection $|\Gamma|$ decreases, see figure 18.

The color scale in both datasets corresponds to the magnitude of the reflection $|\Gamma|$. The characteristic curves and splittings show the transition frequencies of the system. In both datasets, avoided level crossings are visible. Avoided level crossings occur when the qubit and the cavity resonator go into resonance. That is, when the detuning is decreased, the energy levels corresponding to the qubit and the cavity resonator respectively are expected to intersect, but instead they are repelled. This is due to the coupling between the cavity resonator and the transmon, which in the Jaynes-Cummings Hamiltonian (equation (3.6.11)) is determined by g.

To be able to use the experimental data for quantitative analysis, the interesting energy levels had to be extracted from the datasets. The datasets were divided into vertical slices, where each slice correspond to a specific magnetic flux. Then, for each fixed magnetic flux, a Lorentzian was fitted to determine the frequency. A vertical slice and the plotted data is shown in figure 18, where the two magnitude drops correspond to the two curves.

To automate the work of extracting the frequencies, we wrote a script that performed this procedure automatically. The script was written in the data analysis program Igor Pro. Around the level crossings, near the end of each curve, the signal-to-noise ratio is bad and the script did not produce satisfying results. Hence, near the ends we had to do it manually and by visual inspection determine the frequency. In dataset 1, the signal-to-noise ratio was not a big concern, since the manually processed slice and plot revealed a distinguishable peak. However, in dataset 2 where four levels are visible, only two of them could yield distinguishable peaks using the slice and plot process. To be able to extract any data from the faint levels, we did a complete visual inspection and used a photo editor to enhance the contrast.

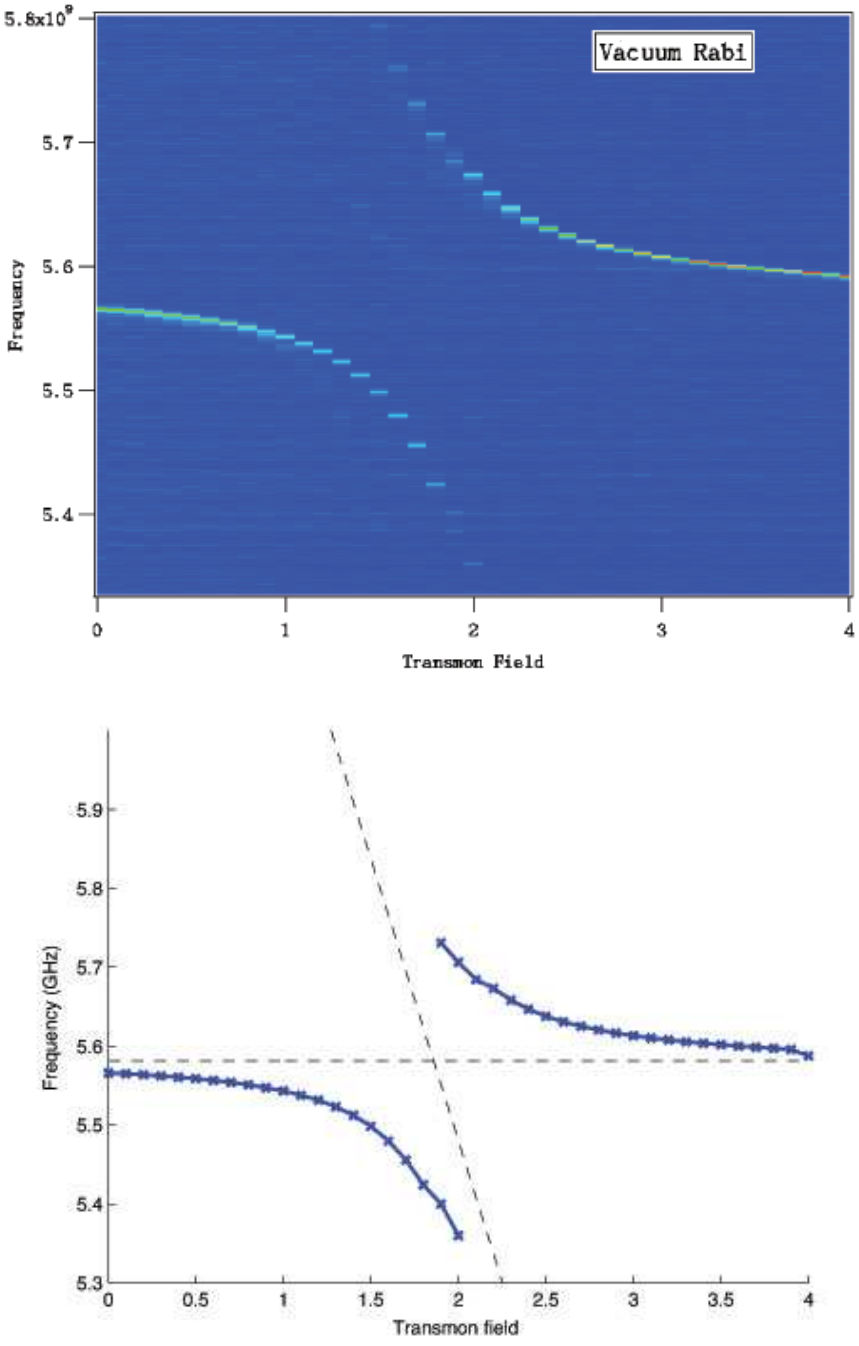

Figure 16: The magnitude of Γ as a function of induced magnetic flux. Note that the magnetic flux has a linear dependence of the inducing current, leading to unknown current units on the x-axis. However, this does not affect the analysis, see section 6.5. The top figure is raw data, where an avoided level crossing is visible. The figure below is the extracted frequency obtained after data reduction. The dashed lines correspond to the uncoupled energy levels of the transmon (steep dashed line) and the cavity resonator (horizontal dashed line). We refer to the measurement data in this image as dataset 1.

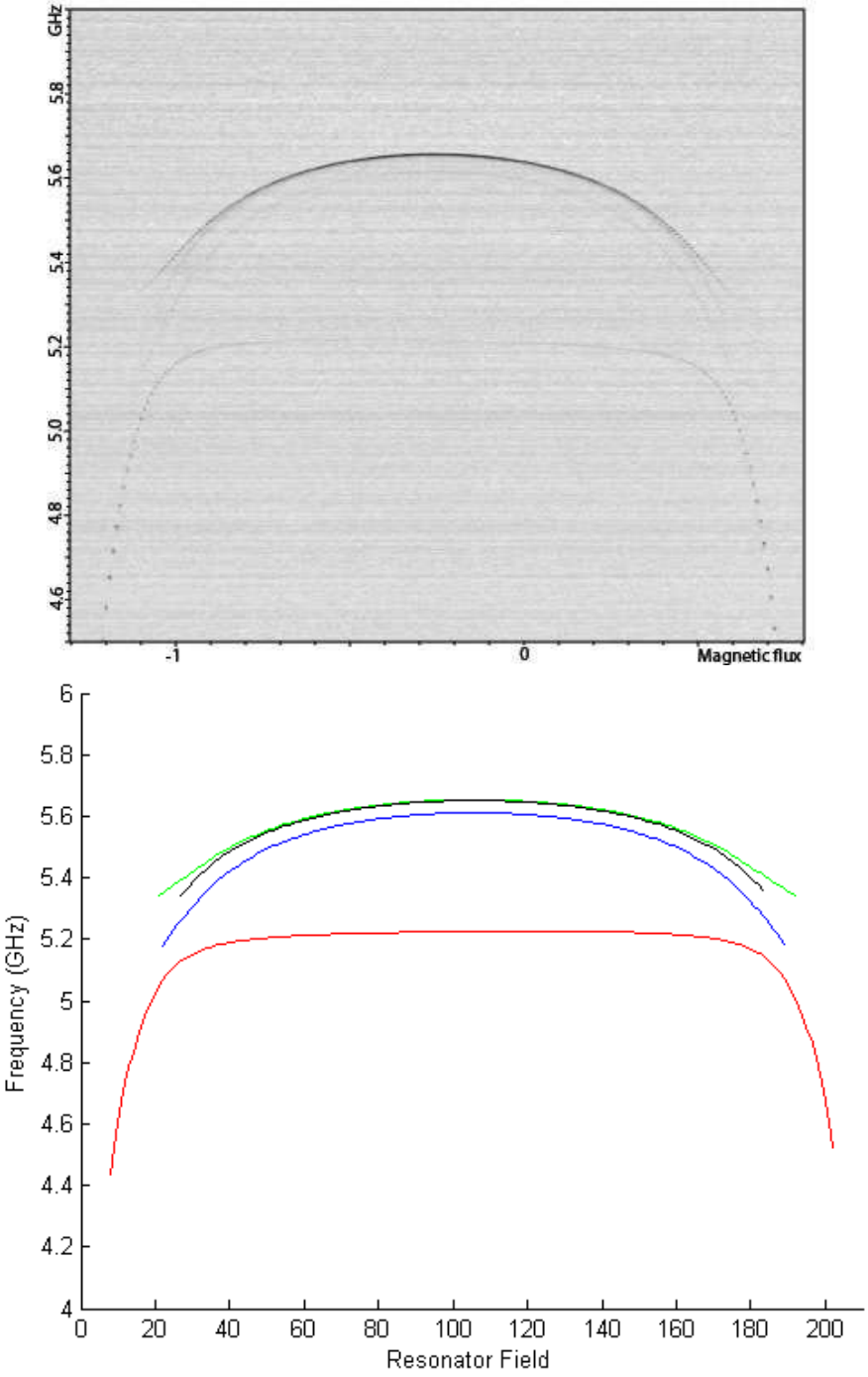

Figure 17: The magnitude of Γ as a function of induced magnetic flux. Note that the magnetic flux has a linear dependence of the inducing current, leading to unknown current units on the x-axis. However, this does not change the analysis, see section 6.5. The flux tunes the cavity and not the qubit, on the contrary to the experiment shown in figure 16. As the cavity and the qubit go into resonance the characteristic avoided level crossings are visible. The two faint levels in between the two distinct levels (the uppermost and lowermost level), correspond to higher excitations. Above is the raw data and below the extracted frequency obtained after data reduction. We refer to the measurement data in this image as dataset 2.

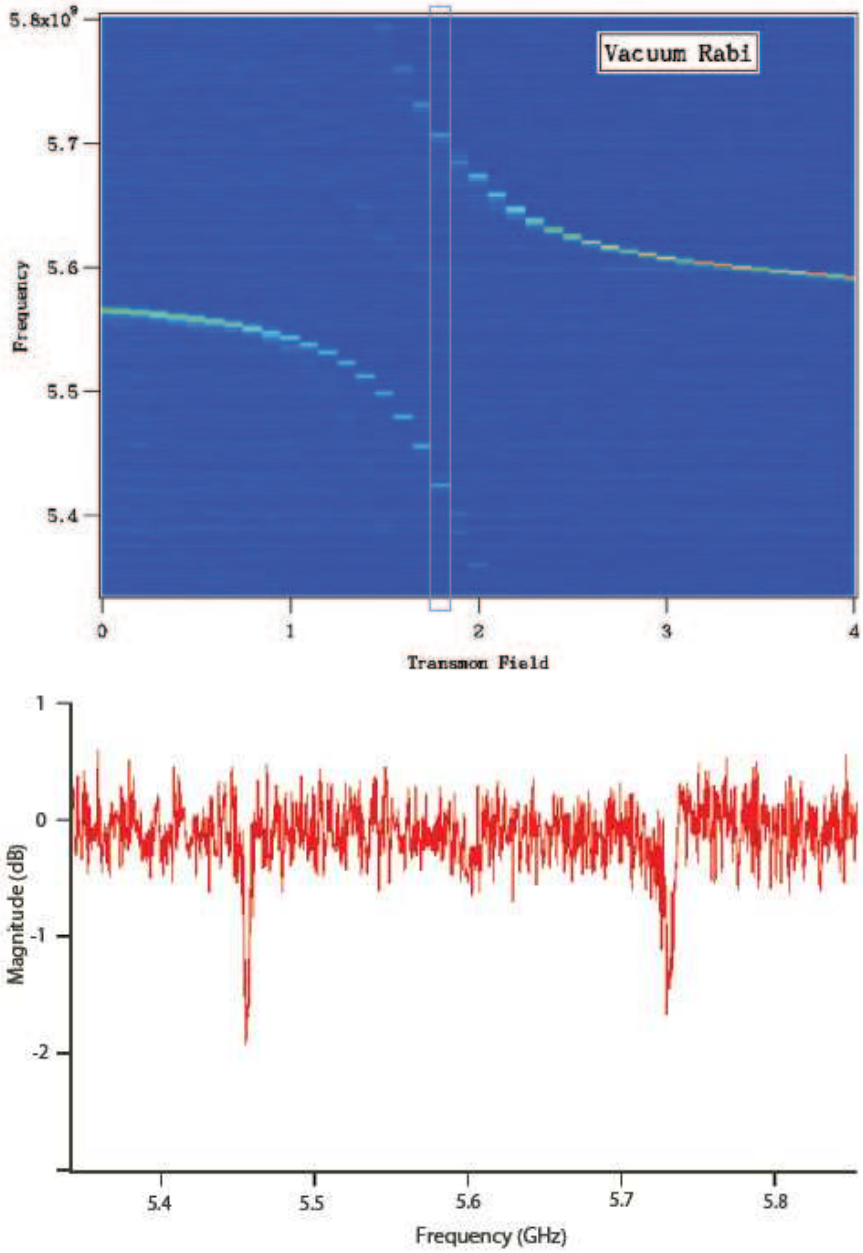

Figure 18: A vertical slice of $|\Gamma|$ (top), the data from that slice plotted as a function of frequency (bottom). The two magnitude drops correspond to the desired frequencies.

6.1 Simulation of a Two-level System in *Matlab*

Section 3.6 contains a derivation of a Hamiltonian for a general qubit in a two-level approximation, that is equation (3.6.11). This does not account for the physical realization of the qubit but just approximates the qubit as a general two-level system. With the Hamiltonian in equation (3.6.11) and the approximate energy difference in the transmon qubit, using equation (5.4.2) together with (5.1.4), we get

$$\hat{H} = \hbar\omega_r \hat{a}^\dagger \hat{a} - \frac{1}{2}\left(\sqrt{8E_{J0}\left|\cos\left(\pi\frac{\Phi}{\Phi_0}\right)\right| E_C} - E_C\right)\hat{\sigma}_z + \hbar g(\hat{\sigma}_+\hat{a} + \hat{\sigma}_-\hat{a}^\dagger), \tag{6.1.1}$$

which is the Hamiltonian used in this section. It is now possible to insert values for the parameters E_{J0}, E_C, g and ω_r and then calculate the eigenvalues of the Hamiltonian. In order to do this we wrote a short *Matlab*script, which calculated the eigenvalues of the Hamiltonian in equation (6.1.1). We choose parameter values that were similar to those of the measured device and the numerical values used to obtain figure 19 are

$$\begin{aligned} \frac{\omega_r}{2\pi} &= 5.6 \text{ GHz}, \\ \frac{g}{2\pi} &= 0.2 \text{ GHz}, \\ \frac{E_{J0}}{E_C} &= 100, \\ \frac{E_{J0}E_C}{h^2} &= 5.8 \text{ GHz}^2. \end{aligned} \tag{6.1.2}$$

In this simulation the values of ω_r and g are determined from looking at figure 16; ω_r is the frequency were the avoided level crossing occurs (the horizontal dashed line) and g is determined from the minimum of the separation of the energy levels. The minimum of the separation is roughly equal to $\frac{g}{\pi}$. $\frac{E_{J0}}{E_C}$ was initially set to 100 (transmon regime) as an educated guess and then some trial and error fitting followed to get a picture like the one in figure 16.

With the current choice of Hamiltonian, we are limited to only two levels for the qubit but it is possible to choose the number of photon states n for the cavity resonator. We found that the lowest eigenvalues did not change for values of $n \geq 5$. In the left of figure 19, the entire spectrum of the lowest eigenvalues is displayed and many avoided level crossings are visible. In the right of figure 19, there is an enlargement of the lowest energy splitting and it is easy to see the resemblance between it and figure 16.

The calculations that were done in this section are all based on the Jaynes-Cummings Hamiltonian in equation (6.1.1) and make a qualitative picture of the transmon qubit.

6.2 Extensions of the Jaynes-Cummings Model

To make a more quantitative model than we did in section 6.1, we need to examine the physical realization of the transmon qubit. In this section, we work with the Hamiltonian in equation (5.4.1), which is derived from the Lagrangian of the circuit diagram of the system. In the transmon qubit, the ratio $\frac{E_J}{E_C}$ is large and we see that the off-diagonal

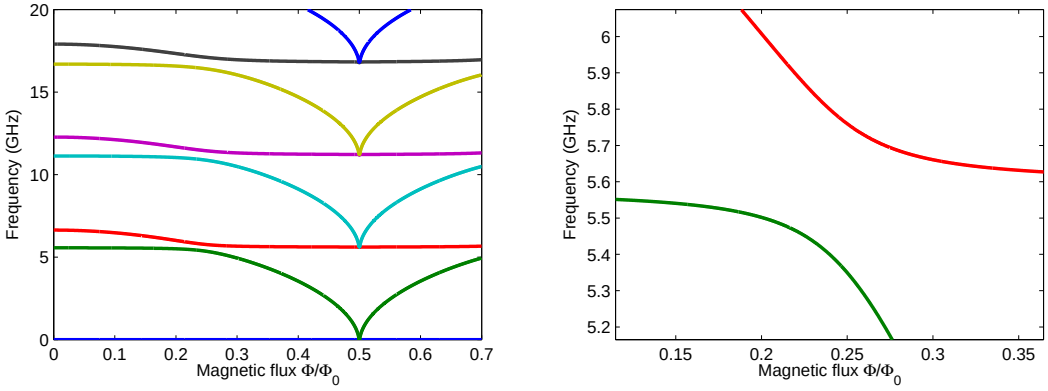

Figure 19: The figure on the left shows the full view of the entire set of calculated energy levels of the transmon qubit within the approximation of equation (6.1.1). The figure on the right is an enlargement of the lowest energy splitting of the left figure. The parameters are set to make the levels correspond roughly to figure 16 and we see that we are able to produce energy splittings which look similar.

elements of the Hamiltonian matrix become large in the charge basis. This makes the charge basis a worse choice of basis than in the CPB case.

The Hamiltonian matrix is infinitely large because it takes into account an unlimited number of Cooper pairs and photons. However, to numerically calculate the eigenenergies of the system, we can only consider a finite number of Cooper pairs and photons, i.e. the Hamiltonian is truncated. It turns out to be convenient to work in the charge basis, since the higher charge states contribute less and less to the eigenenergies. It is possible to simply calculate the eigenenergies with larger and larger Hamiltonian matrices until they converge. We have then found a suitable level of truncation.

From equation (5.4.1), the Hamiltonian of the transmon together with the cavity can be written explicitly with all tensor products (see appendix A for details) as

$$\hat{H}_{\text{tc}} = \underbrace{4E_C(\hat{n}_q - n_g)^2}_{\hat{H}_{\text{CPB1}}} \otimes \hat{\mathbf{1}} - E_J \underbrace{\sum_{n_q=-\infty}^{\infty} \frac{1}{2}\left(|n_q\rangle\langle n_q+1| + |n_q+1\rangle\langle n_q|\right)}_{\hat{H}_{\text{CPB2}}} \otimes \hat{\mathbf{1}} +$$

$$+\hat{\mathbf{1}} \otimes \underbrace{\hbar\omega_r \hat{a}^\dagger \hat{a}}_{\hat{H}_{\text{cavity}}} + \underbrace{2\beta e V^0_{rms} \hat{n}_q \otimes (\hat{a}^\dagger + \hat{a})}_{\hat{H}_{\text{interaction}}}, \tag{6.2.1}$$

where $\hat{\mathbf{1}}$ is the identity matrix. To numerically calculate the eigenvalues of the Hamiltonian we have to write it on matrix form.

The first two terms in equation (6.2.1) are the Hamiltonian of the CPB. The number states for the CPB Hamiltonian are the base vectors in the charge basis $|n_q\rangle$, expressing

n_q extra Cooper pairs on one of the islands and is written as

$$|n_q\rangle = \begin{pmatrix} \vdots \\ 0 \\ 1 \\ 0 \\ \vdots \end{pmatrix}, \langle n_q| = \begin{pmatrix} \dots & 0 & 1 & 0 & \dots, \end{pmatrix} \tag{6.2.2}$$

where the number 1 is in the n_q position in the array, which is of infinite length.

The charge basis forms a complete set (see section 3.1),

$$\sum_{n_q=-\infty}^{\infty} |n_q\rangle\langle n_q| = \hat{\mathbf{1}}. \tag{6.2.3}$$

$\hat{H}_{CPB1}$ in (6.2.1) contains the $\hat{n}_q$ operator, whose eigenvalues in the charge basis denote the number of extra Cooper pairs on the island, $\hat{n}_q|n_q\rangle = n_q|n_q\rangle$. Thus the first term can be expressed as

$$\hat{H}_{\text{CPB1}} = 4E_C(\hat{n}_q - n_g)^2 \cdot \hat{\mathbf{1}} = \sum_{n_q=-\infty}^{\infty} 4E_C(n_q - n_g)^2 |n_q\rangle\langle n_q| \tag{6.2.4}$$

and hence gives the matrix representation:

$$4E_C \begin{pmatrix} \ddots & \vdots & \vdots & \dots & \vdots & \vdots & \iddots \\ \dots & (-n_q - n_g)^2 & 0 & \dots & 0 & 0 & \dots \\ \dots & 0 & (-n_q + 1 - n_g)^2 & \dots & 0 & 0 & \dots \\ \vdots & \vdots & \vdots & \ddots & \vdots & \vdots & \vdots \\ \dots & 0 & 0 & \dots & (n_q - 1 - n_g)^2 & 0 & \dots \\ \dots & 0 & 0 & \dots & 0 & (n_q - n_g)^2 & \dots \\ \iddots & \vdots & \vdots & \dots & \vdots & \vdots & \ddots \end{pmatrix}. \tag{6.2.5}$$

$\hat{H}_{CPB2}$ in the Hamiltonian (6.2.1) is already defined in the charge basis, and thus gives

$$\frac{E_J}{2} \sum_{n_q=-\infty}^{\infty} (|n_q\rangle\langle n_q + 1| + |n_q + 1\rangle\langle n_q|) = \frac{E_J}{2} \begin{pmatrix} \ddots & \vdots & \vdots & \vdots & \dots & \vdots & \vdots & \vdots & \iddots \\ \dots & 0 & 1 & 0 & \dots & 0 & 0 & 0 & \dots \\ \dots & 1 & 0 & 1 & \dots & 0 & 0 & 0 & \dots \\ \dots & 0 & 1 & 0 & \ddots & 0 & 0 & 0 & \dots \\ \vdots & \vdots & \vdots & \vdots & \ddots & \ddots & \vdots & \vdots & \vdots \\ \dots & 0 & 0 & 0 & \ddots & 0 & 1 & 0 & \dots \\ \dots & 0 & 0 & 0 & \dots & 1 & 0 & 1 & \dots \\ \dots & 0 & 0 & 0 & \dots & 0 & 1 & 0 & \dots \\ \iddots & \vdots & \vdots & \vdots & \dots & \vdots & \vdots & \vdots & \ddots \end{pmatrix}. \tag{6.2.6}$$

Moreover, to obtain the matrix representation for the Hamiltonian describing the photons in the cavity, $\hat{H}_{\text{cavity}}$, the same method is applied as for the CPB Hamiltonian. The

number states $|n_c\rangle$ express the number of photons in the cavity resonator and are defined similarly to (6.2.2), but cannot take negative values, i.e. negative number of photons in the cavity. The basis is thus $|n_c\rangle = [0\ \dots\ 0\ 1\ 0\dots]$ and it forms a complete set as the charge basis (6.2.3). Then the annihilation and creation operators gives the off-diagonal matrix elements in the Hamiltonian for the field. Remembering equations (3.5.7), $\hat{a}|n_c\rangle = \sqrt{n_c}|n_c - 1\rangle$ and $\hat{a}^\dagger|n_c\rangle = \sqrt{n_c+1}|n_c+1\rangle$ and using the completeness relation for $|n_c\rangle$, the creation operator is

$$\hat{a}^\dagger \cdot \underbrace{\sum_{n_c=0}^{\infty} |n_c\rangle\langle n_c|}_{=\hat{\mathbf{1}}} = \sum_{n_c=0}^{\infty} \sqrt{n_c+1}|n_c+1\rangle\langle n_c| = \begin{pmatrix} 0 & 0 & 0 & 0 & \dots & 0 & \dots \\ \sqrt{1} & 0 & 0 & 0 & \dots & 0 & \dots \\ 0 & \sqrt{2} & 0 & 0 & \dots & 0 & \dots \\ 0 & 0 & \sqrt{3} & 0 & \dots & 0 & \dots \\ \vdots & \vdots & \vdots & \ddots & \ddots & \vdots & \dots \\ 0 & 0 & 0 & \dots & \sqrt{n_c+1} & 0 & \dots \\ \vdots & \vdots & \vdots & \vdots & \vdots & \ddots & \ddots \end{pmatrix}$$

and the annihilation operator is

$$\hat{a} \cdot \hat{\mathbf{1}} = \sum_{n_c=0}^{\infty} \sqrt{n_c}|n_c - 1\rangle\langle n_c| = \begin{pmatrix} 0 & \sqrt{1} & 0 & 0 & \dots & 0 & \dots \\ 0 & 0 & \sqrt{2} & 0 & \dots & 0 & \dots \\ 0 & 0 & 0 & \sqrt{3} & \dots & 0 & \dots \\ 0 & 0 & 0 & 0 & \ddots & \vdots & \dots \\ \vdots & \vdots & \vdots & \vdots & \ddots & \sqrt{n_c} & \dots \\ 0 & 0 & 0 & 0 & \dots & 0 & \ddots \\ \vdots & \vdots & \vdots & \vdots & \vdots & \vdots & \ddots \end{pmatrix}.$$

In analogy with previous equations, the number operator n_c (see eq.(3.5.8)) is in its matrix representation:

$$\hat{n}_c \cdot \hat{\mathbf{1}} = \sum_{n_c=0}^{\infty} n_c|n_c\rangle\langle n_c| = \begin{pmatrix} 0 & 0 & 0 & 0 & \dots & 0 & \dots \\ 0 & 1 & 0 & 0 & \dots & 0 & \dots \\ 0 & 0 & 2 & 0 & \dots & 0 & \dots \\ 0 & 0 & 0 & 3 & \dots & 0 & \dots \\ \vdots & \vdots & \vdots & \vdots & \ddots & \vdots & \dots \\ 0 & 0 & 0 & 0 & \dots & n_c & \dots \\ \vdots & \vdots & \vdots & \vdots & \vdots & \vdots & \ddots \end{pmatrix}. \tag{6.2.7}$$

The last term in the Hamiltonian (6.2.1), $\hat{H}_{\text{interaction}} = 2\beta e V^0_{rms}\hat{n}_q(\hat{a}^\dagger + \hat{a})$ is the coupling between the cavity and the qubit. Using for respective basis the completeness relation, the coupling term is the tensor product

$$\left(\hat{n}_q \underbrace{\sum_{n_q=-\infty}^{\infty} |n_q\rangle\langle n_q|}_{=\hat{\mathbf{1}}}\right) \otimes \left((\hat{a}^\dagger + \hat{a}) \underbrace{\sum_{n_c=0}^{\infty} |n_c\rangle\langle n_c|}_{=\hat{\mathbf{1}}}\right) =$$

$$= \begin{pmatrix} \ddots & & \vdots & & \cdots & & \vdots & & \iddots \\ & & & & & & & & \\ \cdots & -n_q \begin{pmatrix} 0 & \sqrt{1} & 0 & \cdots \\ \sqrt{1} & 0 & \sqrt{2} & \cdots \\ 0 & \sqrt{2} & 0 & \ddots \\ \vdots & \vdots & \ddots & \ddots \end{pmatrix} & \cdots & & 0 & & \cdots \\ & & & & & & & & \\ \vdots & & \vdots & & \ddots & & \vdots & & \vdots \\ & & & & & n_q \begin{pmatrix} 0 & \sqrt{1} & 0 & \cdots \\ \sqrt{1} & 0 & \sqrt{2} & \cdots \\ 0 & \sqrt{2} & 0 & \ddots \\ \vdots & \vdots & \ddots & \ddots \end{pmatrix} & & \\ \cdots & & 0 & & \cdots & & & \cdots & \\ & & & & & & & & \\ \iddots & & \vdots & & \cdots & & \vdots & & \ddots \end{pmatrix}. \tag{6.2.8}$$

Now with all terms in the Hamiltonian (6.2.1) defined as matrices, the energy eigenvalues are simply the eigenvalues of the matrix, which can be obtained by diagonalization.

6.3 Implementing in *Matlab*

In order to nummerically calculate the eigenenergies of the Hamiltonian (5.4.1) we wrote a function in Matlab. The full program can be seen in Appendix C. The function takes the parameters E_C, E_J, ω_r and $2\beta e V^0_{rms}$ and returns the energy-levels for the Hamiltonian. To simplify, all parameters including eigenenergies are given in GHz.

That leaves the parameter n_g in the Hamiltonian. For a transmon, the exact value of n_g should not affect the energies of the system. However, it should be chosen such that there are roughly as many charge states over and under n_g.

The program first calculates the truncated Hamiltonian matrix. Constructing this in Matlab from equations (6.2.5), (6.2.6), (6.2.7) and (6.2.8) is trivial; the diagonal matrices is constructed by *diag*, and the Kronecker tensor product of pair of matrices is calculated by *kron*. When the Hamiltonian matrix is constructed, its eigenenergies are calculated by *eig*.

The program was made such that the number of charge states for the transmon and photon states in the cavity resonator that the program takes into account can vary. After some experimenting we found that the energies of the lowest eigenstates had converged at $n_{trans} = 15$ and $n_{photons} = 5$. This yield a Hamiltonian with size 75×75. Since this program will be used to fit the parameters of the two datasets it is crucial that it runs sufficiently fast. This makes 15 charge states for the transmon and 5 states for the resonator a good compromise.

6.4 Verification with the Cooper Pair Box

In order to verify that our simulation program, *extendedJaynesCummings.m* (Appendix C), was accurate, a comparison with the theoretical behavior of Cooper pair box was done. The simulation program was set to one cavity state, i.e. zero photons in the cavity, making the last two terms in the transmon Hamiltonian (equation (5.4.1)) zero. This corresponds

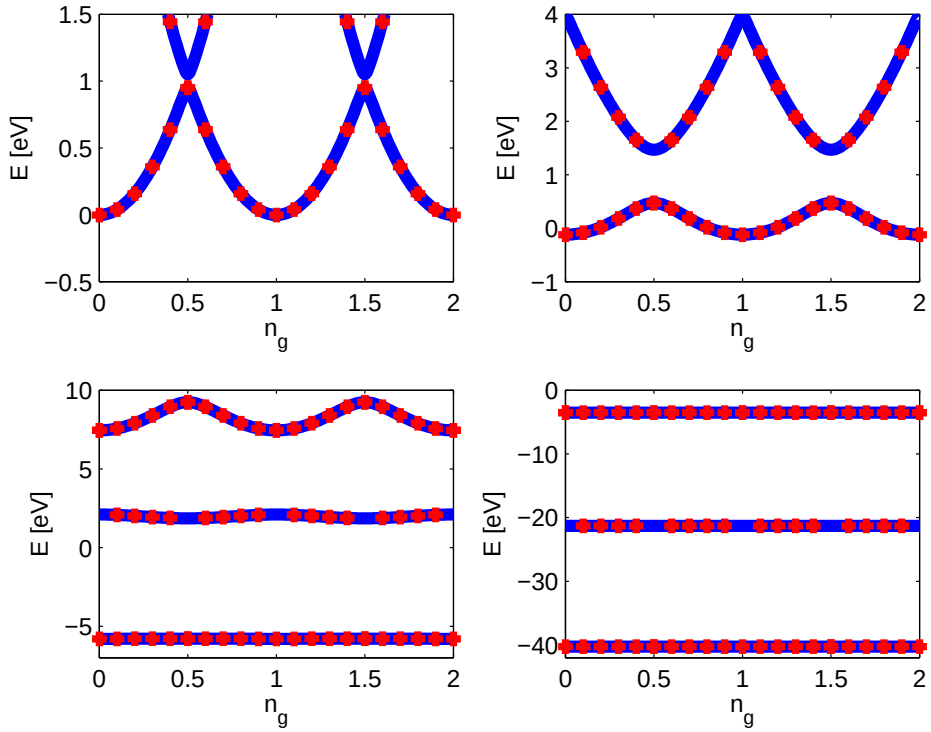

Figure 20: The graphs are representing energy eigenvalues for different ratios between the Josephson energy and the charging energy. In the left corner the ratio is 0.1, the next has $E_J = E_C$, the second row has the ratios 10 and 50. The blue are the numerical values and the red dots are the analytical values. As seen, the numerical and calculated values agree.

to the Cooper pair box (Hamiltonian in equation (5.2.1)). The Schrödinger equation for the CPB is a Mathieu equation [21][31]. We can therefore use Matheiu-characteristics in Mathematica to solve the CPB problem analytically. Both wave functions and eigenenergies can be evaluated but we were only interested in the eigenenergies.

Results from the two methods are featured in figure 20 for four different values of the ratio E_J over E_C. It can be noticed that for a higher value of this ratio, the energy levels become flatter and the gap between different levels grows. It shows also that *extendedJaynesCummings.m* (blue lines) and the analytical method (red dots) resulted in identical values and that *extendedJaynesCummings.m* works properly for the Cooper pair box.

6.5 Fitting of Parameters

6.5.1 Modelling Dataset 1

In the first dataset the cavity resonator is held at a relatively constant frequency while the transmon is tuned by a current x, inducing a magnetic flux through the SQUID in the transmon. Ideally, this current should not affect the cavity resonator. In reality however, we have to take into account that some magnetic flux has leaked into the SQUID in the

resonator. In the small interval of the first avoided level crossing, it should suffice to assume that the resonance frequency depends linearly on x.

Because of stray magnetic fields, zero current does not necessarily correspond to zero magnetic flux. The magnetic flux should however depend on the current as $\Phi/\Phi_0 = kx+m$. Visually estimated from the full measurement that dataset 1 comes from, the transition energy of the transmon is periodic with a period of 15 "current units" and assumes its maximal value for $x = -2$ "current units".

Thus, the parameters in the Hamiltonian (5.4.1) should depend on x as

$$\begin{aligned} E_C, 2\beta e V^0_{rms} \text{ constant}, \\ E_J = E_{J0}|\cos \pi(x+2)/15|, \\ \omega_r = \omega_{r0} + x \cdot \omega_{rslope}. \end{aligned} \tag{6.5.1}$$

For each value of x, we can use *extendedJaynesCummings.m* (see Appendix C) to calculate the energy levels of the system. The two curves in the dataset should correspond to the two lowest transitions from the ground state; adding one photon in the cavity resonator and exciting the transmon to the first excited level or superpositions thereof. Because of this, the lower curve in dataset 1 (figure 16) corresponds to the transition $E_1 - E_0$ and the upper curve should correspond to the transition $E_2 - E_0$.

6.5.2 Modelling Dataset 2

In this dataset the cavity resonator is tuned while the energies for the transmon are constant. This means that all parameters corresponding to the transmon, E_C, E_J, $2\beta e V^0_{ems}$ are constant.

The frequency of the cavity resonator as a function of the magnetic flux is given in [32] as

$$\omega_r = \frac{2\pi f_0}{1 + l/|\cos(\pi\Phi/\Phi_0)|}, \tag{6.5.2}$$

where $l = .05$ was given by our supervisors together with the dataset.

As for the transmon, the magnetic flux controlling the resonance frequency of the cavity resonator should depend linearly on the current, x, i.e. $\Phi/\Phi_0 = k'x + m'$. Though these additional parameters are needed to make a good fit, their exact values are not of interest since they are specific to the dataset.

After putting some typical values for the parameters in *extendedJaynesCummings.m* it is apparent which transitions correspond to each curve in the data. From the lowest curve to the highest curve in figure 17 these transitions are $E_1 - E_0$, $E_4 - E_1$, $E_5 - E_2$ and $E_2 - E_0$.

6.6 Results

Using the models above to describe the two datasets, we estimated the parameters in these models by minimizing the sum of squares of the residuals (errors) between our theoretical curves and the experimental values. The results for both datasets are shown in table 1. Further, the least square fits are shown in figure 21, 22 and 23.

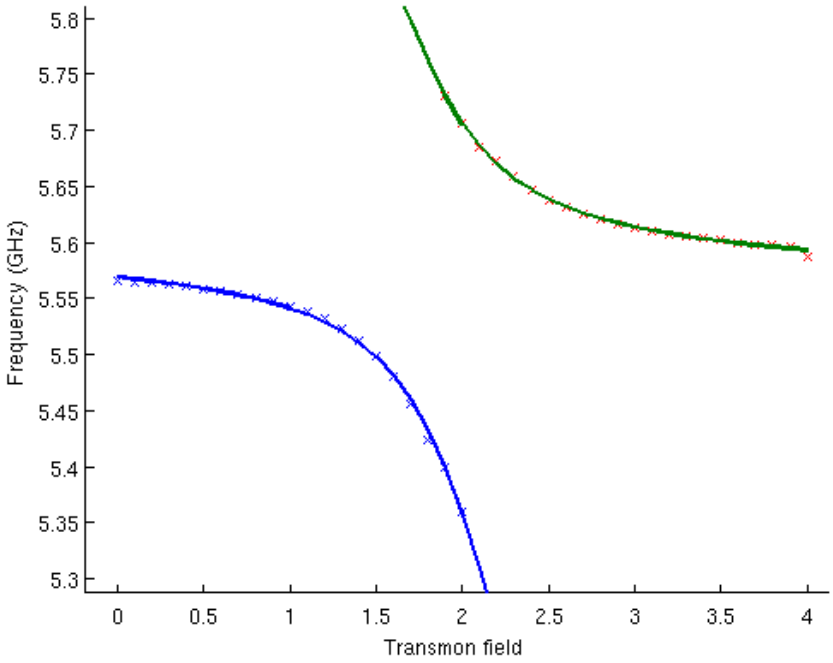

Figure 21: Fitted curves compared to the data in figure 16.

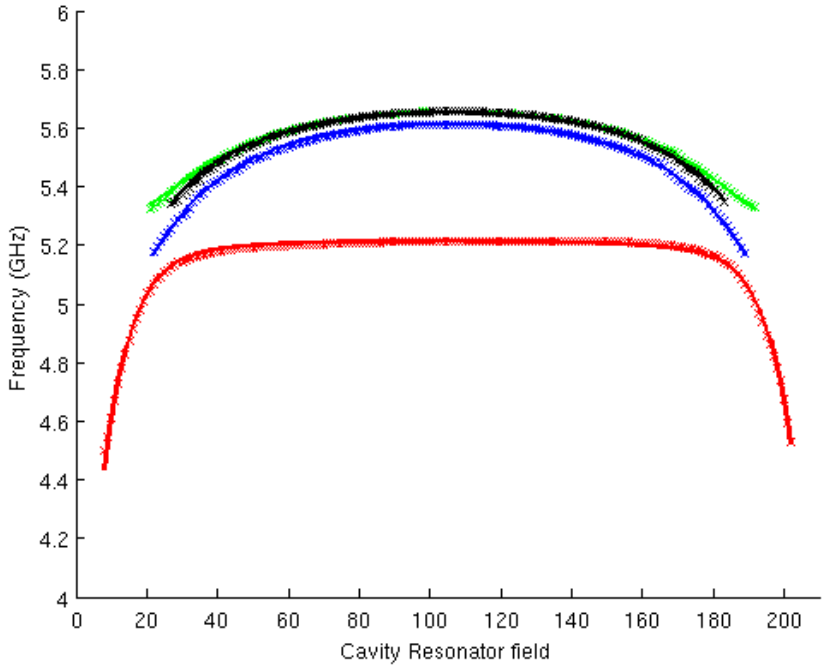

Figure 22: Fitted curves compared to the data in figure 17.

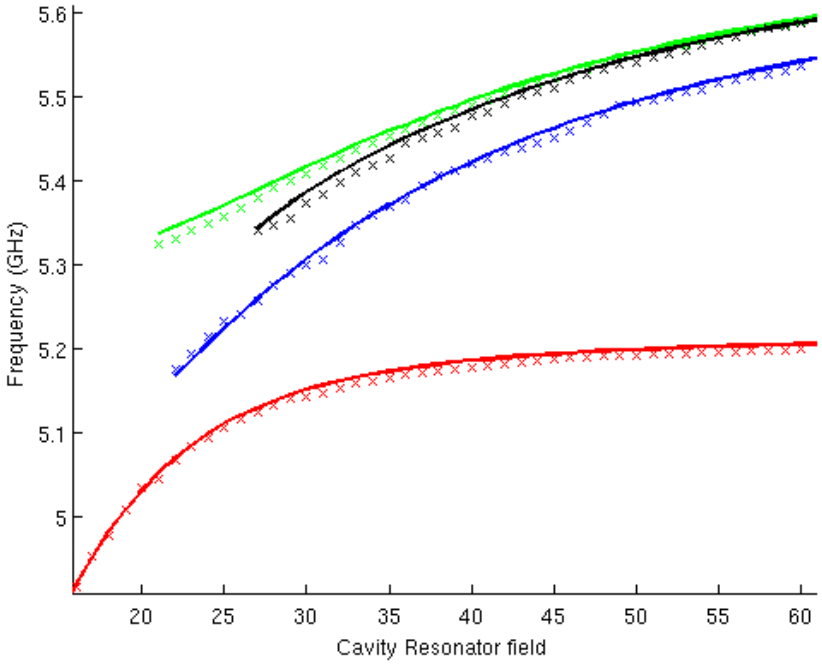

Figure 23: Enlargement of figure 22, where we see the avoided level crossing.

We choose to estimate $E_J E_C$ and $\frac{E_J}{E_C}$ instead of using the values of E_J and E_C directly. The reason for this is that $E_J E_C$ is strongly correlated to the energy difference between the ground state and first excited state for the transmon, which is clearly visible in both datasets. The parameter $\frac{E_J}{E_C}$ describes the anharmonicity of the transmon and is harder to determine since the transition to higher transmon states is not directly visible in any dataset. However, in the second dataset the two faint lines depend on the anharmonicity which should allow us to determine this ratio.

To get confidence intervals for the parameters we used a χ^2-test. This defines a 68 % confidence interval for each parameter as the interval where the parameter can be chosen such that that

$$\chi^2 = \sum_i \frac{(y(x_i) - y_i)^2}{\sigma_i^2} \tag{6.6.1}$$

differs by at most one from its lowest value [33]. The sample variance, σ_i^2, was estimated as the sum of squares of the residuals for the best fit divided by $N - k$, the number of data points minus the number of parameters.

Using the extracted parameters from dataset 2, an energy diagram of the measured system can be constructed. This can be seen in figure 24. As a comparison, the corresponding energy diagram without the coupling is shown in figure 25. From these, we can identify the different energy transitions and see the effects of the coupling.

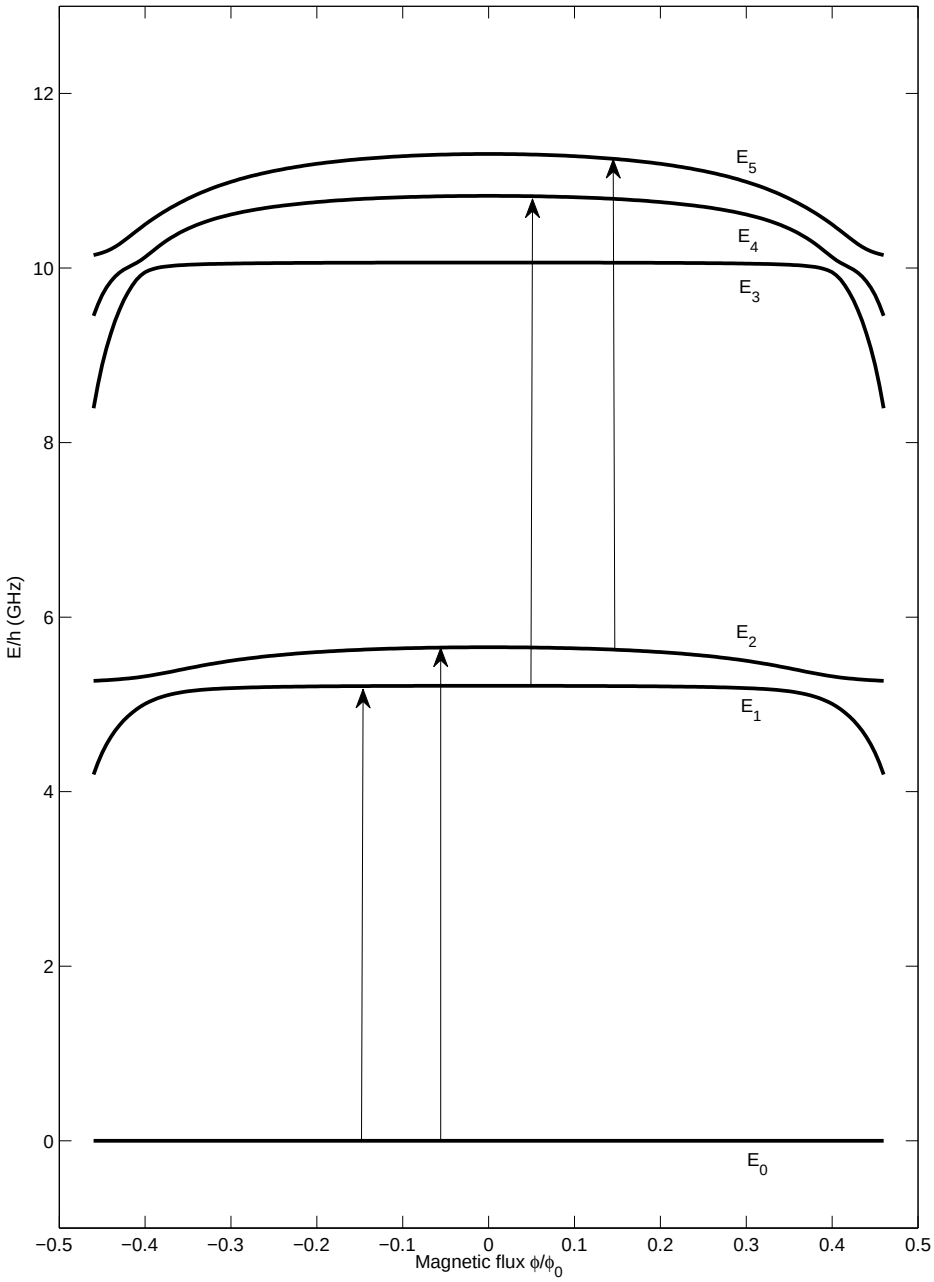

Figure 24: Energy diagram for the coupled transmon and cavity resonator where the resonator frequency is tuned by a magnetic flux. The four arrows in the diagram shows the observed transitions in dataset 2.

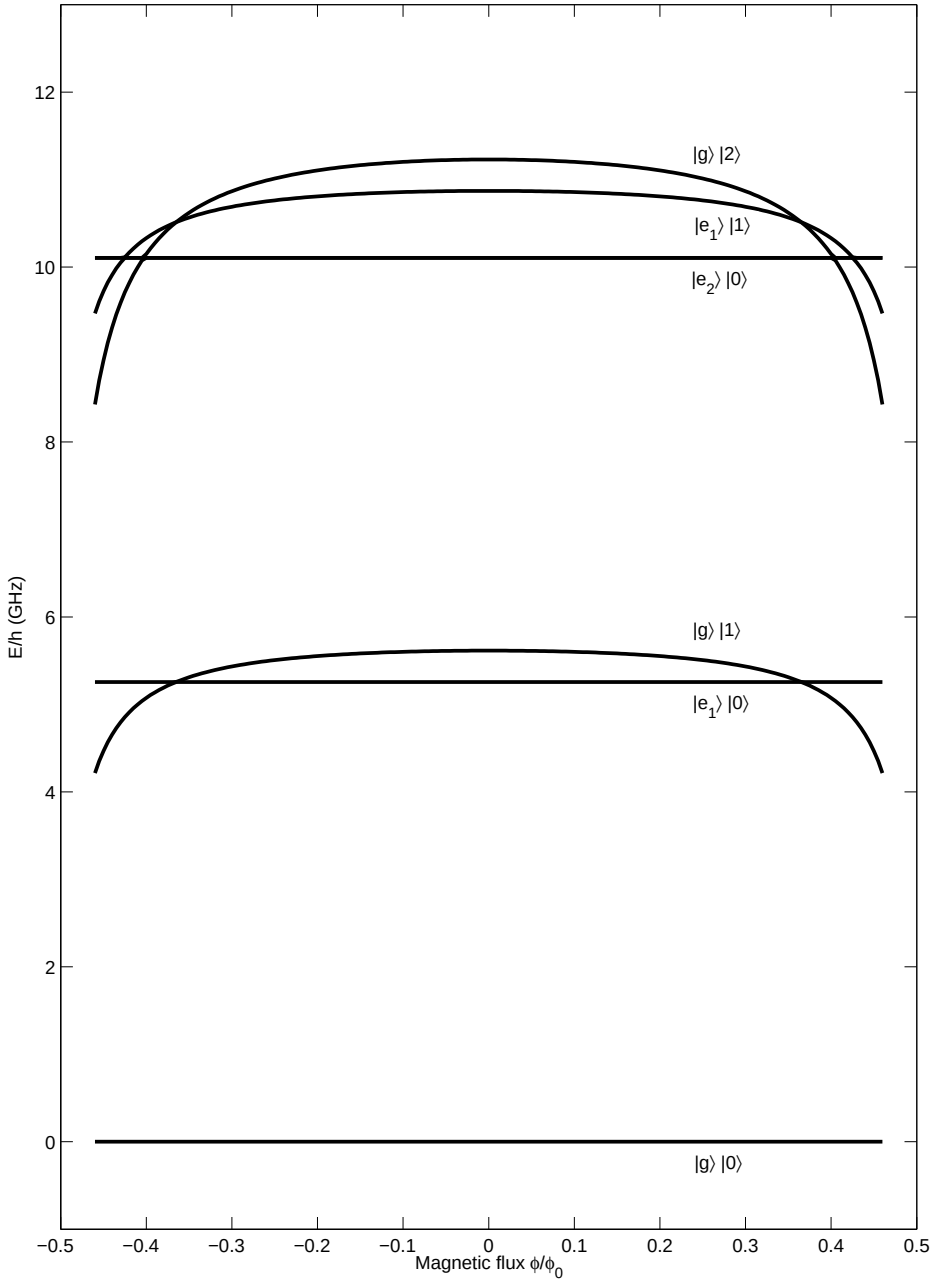

Figure 25: Energy diagram for the transmon and cavity resonator without the coupling term. $|g\rangle$ denotes the ground state, $|e_n\rangle$ the n:th excited state for the transmon and $|m\rangle$ the number of photons in the cavity. The resonator frequency is tuned by a magnetic flux. Note that, at each point where two energies cross, the coupling (see figure 24) will act to make the curves repel and they will gradually turn into each other.

Table 1: Extracted parameters from dataset 1 and 2, given with 68 % confidence interval.

	Dataset 1			Dataset 2	
$2\beta eV^0_{rms}/h$	0.125 ± 0.040	(GHz)	$2\beta eV^0_{rms}/h$	0.1301 ± 0.00095	(GHz)
$E_{J0} \cdot E_C/h^2$	6.024 ± 0.357	$(\text{GHz})^2$	$E_J \cdot E_C/h^2$	3.9465 ± 0.0075	$(\text{GHz})^2$
E_{J0}/E_C	150 ± 100	-	E_J/E_C	34.5644 ± 0.9456	-
$\omega_r/2\pi$	5.60775 ± 0.00095	(GHz)	f_0	5.8953 ± 0.0006	(GHz)

7 Discussion

For being a thesis in the field of quantum computers it has covered next to none of the applications. For example one could look in to the algorithm part, where we find quantum teleportation, Shor's algorithm and quantum error correction. Shor's algorithm for factorizing numbers, Grover's search algorithm and simulating quantum systems are, at present, the only really useful algorithms were quantum computers outperforms classical computers. The reason for not considering these applications is that today the superconducting qubit technology is far from implementing useful algorithms.

In the beginning the project was unspecified and we were allowed to choose what we wanted to do within the field of quantum computation and quantum information. We chose a combined project of literature studies and data analysis. In retrospect, some of the literature studies that we did, we were unable to implement in the data analysis. If we had focused more on the appropriate theory we would have been able to either do more complex derivations and/or more data analysis. Another option would have been to do a complete literature study and extend Theory - Part II.

The uncertainties, on the parameters we extracted, have large discrepancies between the two datasets even though the datasets come from the same qubit. The values on the parameters themselves also differ because the devices are tuned in different ways for the two measurements. The only parameter not tuned is $2\beta eV^0_{rms}$ and it can be seen in table 1 that it agrees between the two datasets. We can see from the parameter fitting in dataset 1 that it is underconstrained, because it only shows the two lowest transitions in the system. A concern about dataset 1 is that in equation (6.5.1) there are two parameters that have been visually estimated and the uncertainty in these values are not accounted for in the final error analysis. This is largely due to our inexperience concerning error analysis in general. Even though the concerns in dataset 1, it worked out well to fit the theories to both datasets, which shows that our "extended" model is an accurate approximation of the cavity-qubit behavior.

The main problem in quantum computing at present is the decoherence times. It is now possible to construct relatively "good" single qubits, but there is a problem with getting them to work together as they need to be doing in a processor. At present ~ 10 qubits have been successfully coupled and to be able surpass current classical computers ~ 40 qubits need to be coupled.

What is the future of quantum computation using superconducting qubits then? Since macroscopic quantum coherence was shown, the progress in research has been immense, improving decoherence times from ~ 1 ns to ~ 10 μs in just ten years. As mentioned

in the introduction, the superconducting qubit is a promising candidate for a quantum computer, but there are still technological obstacles. Mainly the decoherence times need to be improved but also the read-out needs to be more accurate.

The question really is whether superconducting qubits will be usable to perform quantum computation or not. Today, there is no answer; there are too many issues left [34]. Of course time will tell, but the general consensus within the research community is that superconducting qubits are at least a very promising candidate. One thing is certain, it will not go unnoticed.

Acknowledgements

The central point in this thesis has been theoretical, with many new areas of science. The work has been highly rewarding and gave us a greater insight in many new subjects. This is much thanks to our supervisors who have been most helpful and explained theoretical topics to us even though at times we tried their patience. A big thank you to Chris and Göran!

Thilo Bauch who co-lectured with Göran in Quantum Informatics was also a big help and answered our questions with enthusiasm.

We would also like to thank Anton Frisk Kockum who does his master thesis in the same field as this report and took the Quantum Informatics course with us. He really took time and tried to help us with all the new things that popped up during the course.

We would like to conclude with two qoutes:

> ”The question is not what coherence is, but rather what is **not** coherence”
>
> Göran Johansson when asked in class what coherence really is.

> ”There is various funny stuff going on”
>
> Chris Wilson about dataset 1.

Tommy, Håkan, Anders, Ida-Maria, Tobias
May 2010

Appendix

Appendix A Tensor Product

A and B are two 2 by 2 dimensional complex valued matrices

$$A = \begin{pmatrix} a_{11} & a_{12} \\ a_{21} & a_{22} \end{pmatrix},$$

$$B = \begin{pmatrix} b_{11} & b_{12} \\ b_{21} & b_{22} \end{pmatrix}.$$

The tensor product is then defined as

$$A \otimes B = \begin{pmatrix} a_{11}\begin{pmatrix} b_{11} & b_{12} \\ b_{21} & b_{22} \end{pmatrix} & a_{12}\begin{pmatrix} b_{11} & b_{12} \\ b_{21} & b_{22} \end{pmatrix} \\ a_{21}\begin{pmatrix} b_{11} & b_{12} \\ b_{21} & b_{22} \end{pmatrix} & a_{22}\begin{pmatrix} b_{11} & b_{12} \\ b_{21} & b_{22} \end{pmatrix} \end{pmatrix} = \begin{pmatrix} a_{11}b_{11} & a_{11}b_{12} & a_{12}b_{11} & a_{12}b_{12} \\ a_{11}b_{21} & a_{11}b_{22} & a_{12}b_{21} & a_{12}b_{22} \\ a_{21}b_{11} & a_{21}b_{12} & a_{22}b_{11} & a_{22}b_{12} \\ a_{21}b_{21} & a_{21}b_{22} & a_{22}b_{21} & a_{22}b_{22} \end{pmatrix}.$$

Tensor product is equivalent for higher dimensions. Another handy equality is

$$(A \otimes B)(|\psi_1\rangle \otimes |\psi_2\rangle) = (A|\psi_1\rangle) \otimes (B|\psi_2\rangle).$$

The tensor product is a way to combine two vector spaces into a larger one. This is used to understand multiparticle systems. It can also be referred to as the Kronecker product [35]. Usually tensor products are not explicit marked in quantum physics.

Appendix B Gauge Transformation for the Electromagnetic Field

From Maxwells equations, [14], the electric and the magnetic field can be expressed as

$$\mathbf{E} = -\nabla V - \partial_t \mathbf{A},$$

$$\mathbf{B} = \nabla \times \mathbf{A}.$$

Now if $\mathbf{A}$ undergoes the transformation

$$\mathbf{A} \longrightarrow \mathbf{A} + \nabla\chi.$$

The magnetic field $\mathbf{B}$ will remain the same

$$\mathbf{B} = \nabla \times \mathbf{A} = \nabla \times (\mathbf{A} + \nabla\chi) =$$

$$= \nabla \times \mathbf{A} + \nabla \times \nabla\chi = \nabla \times \mathbf{A},$$

because the curl of the gradient of any scalar field will vanish. In order to leave $\mathbf{E}$ unaffected, one have to make the following transformation

$$\mathbf{E} = -\nabla V - \partial_t \mathbf{A} = -\nabla V - \partial_t (\mathbf{A} + \nabla\chi) =$$

$$= -\nabla (V + \partial_t \chi) - \partial_t \mathbf{A}.$$

The necessary transformation is hence

$$V \longrightarrow V - \partial_t \chi.$$

Appendix C extendedJaynesCummings.m

```
function Etot = extendedJaynesCummings(EJ, EC, Eres, g);

  nresonator        = 5;    % Number of states to account for
  ntransmon         = 15;

  ng = floor(ntrans/2);


  Htot = kron(...
               4*EC*diag( ((0:ntransmon-1)-ng).^2 )...
               -EJ/2*(diag(ones(ntransmon-1,1),1)+diag(ones(ntransmon-1,1),-1))...
            ,...
               eye(nresonator)...
         )...
         +...
         Eres*kron(...
               eye(ntransmon)...
            ,...
               diag(0:nresonator-1)
         )...
         +...
         g*kron(...
               diag( 0:ntransmon-1)...
            ,...
               diag(sqrt(1:nresonator-1),1)+diag(sqrt(1:nresonator-1),-1)...
         );

  Etot = eig(Htot);
  Etot = Etot-Etot(1);
```

References

[1] P.W. Shor. Algorithms for quantum computation: Discrete logarithms and factoring. In *ANNUAL SYMPOSIUM ON FOUNDATIONS OF COMPUTER SCIENCE*, volume 35, pages 124–124. Citeseer, 1994.

[2] I. Chuang M. Nielsen. *Quantum Computing and Quantum Information*. Cambridge University Press, 2000.

[3] G.Johansson and T. Bauch. Lecture notes, Quantum Informatics (FKA172). A gathering of the lecture notes of the curse on http://mina4-49.mc2.chalmers.se/∼gojo71/KvantInfo.html, 2010.

[4] Yu. Pashkin Y. Nakamura and J.S. Tsai. Coherent control of macroscopic quantum states in a single-Cooper-pair box. *Nature*, 398:786–788, 1999.

[5] G. Wendin and V.S. Shumeiko. Superconducting quantum circuits, qubits and computing. http://arxiv.org/PS_cache/cond-mat/pdf/0508/0508729v1.pdf 2010-04-14.

[6] J. Koch, T.M. Yu, J. Gambetta, AA Houck, DI Schuster, J. Majer, A. Blais, MH Devoret, SM Girvin, and RJ Schoelkopf. Charge-insensitive qubit design derived from the Cooper pair box. *Physical Review A*, 76(4):42319, 2007.

[7] P.L. Knight C.C. Gerry. *Introductory quantum optics*. 2000.

[8] J. J. Sakurai. *Modern Quantum Mechanics*. Addison Weasly inc, 1993.

[9] Ian Glendenning. The bloch sphere, 2005. http://www.vcpc.univie.ac.at/∼ian/hotlist/qc/talks/bloch-sphere.pdf 2010-03-18.

[10] http://thermowiki.epfl.ch/tqi/documents/images/cours/sphere_bloch.jpg 2010-03-18.

[11] I. I. Rabi. Space quantization in a gyrating magnetic field. *Phys. Rev.*, 51(8):652–654, April 1937.

[12] R.W. Robinett. *Quantum Mechanics*. Oxford University Press, 1997.

[13] A. Abragam. *The Principles of Nuclear Magnetism*. Oxford University Press, 2002.

[14] David K.Cheng. *Fundamentals of Engineering Electromagnetics*. Addison-Wesley Publishing Company, 1993.

[15] JI Cirac and P. Zoller. Quantum computations with cold trapped ions. *Physical Review Letters*, 74(20):4091–4094, 1995.

[16] University of Innsbruck. http://heart-c704.uibk.ac.at/, 2010-04-29.

[17] A. Villar P. Schindler M. Chwalla M. Riebe C. F. Roos H. Häffner W. Hänsel M. Hennrich R. Blatt T. Monz, K. Kim. Realization of Universal Ion Trap Quantum Computation with Decoherence Free Qubits. *Phys. Rev.*, September 2009.

[18] L.M.K. Vandersypen, M. Steffen, G. Breyta, C.S. Yannoni, M.H. Sherwood, and I.L. Chuang. Experimental realization of Shor's quantum factoring algorithm using nuclear magnetic resonance. *Nature*, 414(6866):883–887, 2001.

[19] J.Q. You and Franco Nori. Superconducting Circuits and Quantum Information. *PHYS.TODAY*, 58:42, 2005.

[20] C. Kittel. *Introduction to Solid State Physics*. John Wiley & Sons, 2005.

[21] M. Sandberg. *Fast-tunable resonators and quantum electrical circuits*. PhD thesis, Chalmers University of Technology, 2009.

[22] John L. Safko H. Goldstein, Charles P. Poole. *Classical Mechanics*. Addison Wesley Publishing Company, 3rd edition, 2002.

[23] BD Josephson. The discovery of tunnelling supercurrents. *Reviews of Modern Physics*, 46(2):251–254, 1974.

[24] M. Tinkham. *Introduction to Superconductivity*. McGraw-Hill, NY, 2nd edition, 1996.

[25] Benjamin S. Palmer. Quantum Computing with a Cooper-Pair Box. http://www.lps.umd.edu/Quantum%20Computing%20Group/Cooper-Pair%20Box%20Qubit/Cooper-PairBoxQubit1.html 2010-03-22.

[26] V. Bouchiat, D. Vion, P. Joyez, D. Esteve, and MH Devoret. Quantum coherence with a single Cooper pair. *Physica Scripta*, 76:165–170, 1998.

[27] R. Johansson. *Quantum mechanics in superconducting electrical circuits and nanomechanical devices*. PhD thesis, Chalmers University of Technology, 2009.

[28] John M. Martinis, S. Nam, J. Aumentado, and C. Urbina. Rabi oscillations in a large josephson-junction qubit. *Phys. Rev. Lett.*, 89(11):117901, Aug 2002.

[29] G. Blatter, V.B. Geshkenbein, and L.B. Ioffe. Design aspects of superconducting-phase quantum bits. *Physical Review B*, 63(17):174511, 2001.

[30] http://www.pi.uni-karlsruhe.de/ustinov/group_hp/fluxon.physik.uni-erlangen.de/pages/opportunities/index.html 2010-03-24.

[31] A. Wallraff M.H. Devoret and J.M. Martinis. Superconducting qubits: A short review. February 2008.

[32] Martin Sandberg, Chris Wilson, Fredrik Persson, Thilo Bauch, Göran Johansson, Vitaly S. Shumeiko, Tim Duty, and Per Delsing. Tuning the field in a microwave resonator faster than the photon lifetime. *Applied Physics Letters*, 92:20, 2008.

[33] D. Keith Robinson Philip R. Bevington. *Data Reduction and Error Analysis*. McGraw-Hill, 3rd edition, 2003.

[34] John Clarke and Frank K. Wilhelm. Superconducting quantum bits. *Nature*, 453(7198):1031–1042, June 2008.

[35] ZS Sazonova and R. Singh. Kronecker product/Direct product/Tensor product in Quantum Information theory. *Arxiv preprint quant-ph/0104019*, 2001.